Absorption Selected Galaxies Along the Line of Sight to GRBs

Christina Henriksen

Master Thesis

Dark Cosmology Centre - Niels Bohr Institute
Copenhagen University

Supervised by Johan P. U. Fynbo

December 2007

Abstract

The purpose of my thesis was to search for the galaxy counterpart of strong MgII absorption systems seen in the spectra of GRBs. Previous studies might have overlooked a whole population of faint galaxies at small impact parameters for MgII absorption systems in QSOs because of its bright glare. With the afterglows of GRBs fading a way, a clear sightline makes deep spectroscopy at small impact parameters possible.

My work was on the three fields of GRB021004, GRB030226 and GRB020813 as these both showed strong MgII absorption as well as had several candidates for the absorbing galaxy within a small impact parameter. I used spectroscopic data from FORS2 at the ESO VLT and I reduced and calibrated the raw data as well as analyzed the combined science frames. I was able to find galaxy counterparts in two absorption systems based on [OII] emission, one in GRB021004 and one in GRB020813. Both of the systems were at a small impact paramter, with the lowest for the galaxy in GRB020813 of only 4.5" from the GRB and thus I have been able to find possible absorbers at a small impact parameters.

Acknowledgements

First of all I would like to thank Johan P. U. Fynbo for being a great supervisor and for always giving me valuable answers, suggestions and friendly advice. My deep gratitude to Johannes Andersen for proofreading and good insights as well as for believing in me and to Anja C. Andersen for moral support in a time where I needed it the most.

Big thanks to Camilla and Rikke for their help and understanding. You mean the world to me.

Finally, I would like to thank my family; My Mom, Dad, and Berit for their invaluable support during my studies and especially during the process of this thesis.

Morten, thank you for bringing joy and happiness into my life.

Contents

Preface

The QSOs was discovered in the 60ies and along with this began the study of absorption selected objects, e.g. MgII, CIV and damped Lyα absorbers. From the beginning the question of how absorption selected objects are related to emission selected objects, i.e. visible galaxies with emission lines from e.g. [OII], was raised, but this question has not yet found a clear answer. Based on studies of QSO sightlines, it has been argued that MgII absorption seen in the spectra of the QSO is related to large (several tens of kpc) extended gaseous halos of luminous galaxies. However, galaxies might have been misidentified as a counterpart to the absorbers, since it has been impossible to detect faint galaxies at small impact parameters, due to the bright glare of the QSO. The optical afterglows of Gamma Ray Bursts offer an unique solution to this problem. Absorption systems can be identified in the spectra of afterglows, and as the afterglows fade away, a deep search for associated galaxies can be carried out. Thus, we are now able to find out whether the MgII absorption might be due to much smaller halos around faint galaxies at small impact parameters instead.

The purpose of my thesis is to search for galaxies associated with MgII absorption in GRB afterglows, in order to determine whether previous studies might have overlooked a population of faint galaxies at low impact parameters. I will study the fields of GRB021004, GRB030226, GRB020813 as well as GRB. All of these GRBs show MgII absorption, and have several faint galaxies at impact parameters of < 5", which might be associated with the absorption systems.

The outline of my thesis is as follows: I will begin with an introduction, covering the theoretical background of my thesis; in particular the theory behind absorption systems and what can be inferred from QSO and GRB sightlines. In chapter 2, I will describe the GRB fields chosen for my thesis. This thesis is based on spectroscopic data from FORS2 at VLT and a major part was the image reduction, calibration and analysis of these. I will therefore outline the observational setup and explain the calibration methods and how these were performed in chapters 3 and 4. Chapter 5 contains the results of my thesis and finally, I will in chapter 6, conclude my thesis and give a summary and an outlook for future research.

Christina Henriksen

December 2007

Chapter 1

Introduction

Our Universe began with the Big Bang. In the beginning it consisted of a hot and dense primordial soup where particles and radiation were in almost thermal equilibrium. After about 10^{-34} s, inflation set in, expanding the Universe exponentially. It ended approx. 10^{-32} s efter the Big Bang, returning The Universe to a radiation-dominated expansion. The Universe cooled rapidly and when it was about 1 s old, the neutrinos were able to decouple from the neutrons and protons and hereby "froze" the neutron to proton ratio, leaving approx. one neutron for every five protons (Ryden 2003). This ratio slowly decreased as the neutrons decayed by weak interactions. After the neutrino freeze-out, the neutrons and protons could interact and form the light elements from deuterium to helium, as well as a small amount of lithium and beryllium. This "Big Bang Nucleosynthesis" ended when the Universe was about 10 min old (Ryden 2003). The Universe went from being radiation-dominated to be matter-dominated after $\approx$ 50,000 years corresponding, to a redshift of $z \approx 3,500$ (Ryden 2003). Redshift is a measure of how much the wavelength of an emitted photon is stretched on the way to us due to the expansion of the Universe, and is thus a measure of time since it was emitted.

At a redshift of $z \approx 1,100$ the epoch of recombination took place where the electrons in the pregalactic gas recombined with ions to form neutral atoms. As a consequence, photons were able to escape freely without being Thomson scattered off the electrons, i.e. the photons were decoupled from the electrons and the Universe became transparent. This happened at a redshift of $\approx 1,000$ and marks the last scattering surface (Longair 1998). Due to the expansion of the Universe the photons were stretched into the microwave region, and we see this today as the Cosmic Microwave Background Radiation (CMB), distributed uniformly across the sky with an almost perfect black-body spectrum with a temperature of 2.725K $\pm$ 1mK (Ryden 2003). The CMB also contains small temperature fluctuations caused by primeval density inhomogeneities at the time of recombination which, have left their imprint on the last scattering surface. These small density inhomogeneities containing cold dark matter turned into the large scale stuctures that we see today, i.e. galaxies, clusters of galaxies, superclusters and empty voids in between.

The first stars were formed by the gravitational collapse of cloud fragments. This probably occurred at around $z \approx 20$ (Stahler & Palla 2004). Since no metals were present, the first stars became very massive due to their inefficient way of cooling. These stars therefore had a short lifetime before exploding as supernovae hereby enriching the interstellar medium. Around $z \approx 10$ the Universe went through an epoch of reionization, where the intergalactic medium was largely ionized by UV emission from e.g. the first stars and quasars. This epoch marks the transition from the cosmic Dark Ages to the moment of galaxy formation, and it is believed to have ended at $z \approx 6$ (Alvarez & Abel 2007). New stars continued to form and galaxies and clusters of galaxies evolved - the Universe evolved into the Universe we see today.

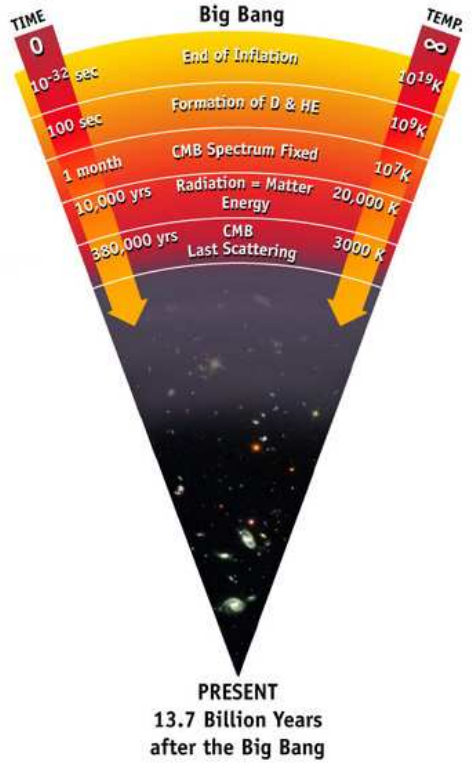

Figure 1.1: Schematic timeline of the Big Bang

1.1 Formation of Structure

On large scales, i.e. larger than approx. 100 Mpc, the Universe is homogeneous and isotropic. On smaller scales, however, the Universe has density fluctuations as it contains stars, galaxies, clusters of galaxies as well as voids. The main theory of structure formation is that small energy density fluctuations in the early Universe were amplified by gravitational instabilities i.e. Jeans instability. These density fluctuations were generated when the Universe went through inflation as small quantum fluctuations in the inflation field expanded with the inflation.
Usually the density fluctuations are represented by the dimensionless:

$$\delta(\vec{r},t) = \frac{\varepsilon(\vec{r},t) - \overline{\varepsilon}(t)}{\overline{\varepsilon}(t)},$$

where $\overline{\varepsilon}$ is the spatially averaged energy density. This means that the density fluctuation is negative in underdense regions and positive in overdense regions. When the fluctuations remain small, i.e. $|\delta| \ll 1$, linear perturbation theory can be used to see how small density fluctuations can grow in amplitude with time under the influence of gravity. The density pertubations grow according to (Ryden 2003):

$$\ddot{\delta} + 2H\dot{\delta} - \frac{3}{2}\Omega_m H^2 \delta = 0.$$

For a multiple-component universe however, δ represent the fluctuation of matter only. The term $2H\dot{\delta}$ is the so-called Hubble-friction term as it slows down the growth of perturbations when the Universe expands. It is not until the Universe becomes matter-dominated that the density perturbations grow in amplitude. When the overdensity reaches $\delta \sim 1$, the linear perturbation

theory breaks down. To solve this, numerical simulations are used instead. They have shown that when $\delta \sim 1$, the overdense region collapses and becomes stable and gravitationally bound. The baryonic matter within this dense region will fall to the center while radiating energy away and form stars and galaxies. If the Universe only consisted of baryonic matter, this would have meant that the density pertubations could not have started to grow before the decoupling at $z \approx 1,000$. However the dominant form of matter in the Universe is dark matter and the density perturbations could then start to grow when the Universe became matter-dominated at $z \approx 3,500$. When decoupling took place, the baryons fell into already existing gravitational wells made by the dark matter.

Another way to look at the pertubations is by means of the power spectrum. To derive this δ is first expressed in terms of Fourier components. The density fluctuation field can be written as (Ryden 2003):

$$\delta(\vec{r}) = \frac{V}{(2\pi)^3} \int \delta_{\vec{k}} e^{-i\vec{k}\cdot\vec{r}} d^3k,$$

where each Fourier component is given by

$$\delta_{\vec{k}} = \frac{1}{V} \int \delta(\vec{r}) e^{i\vec{k}\cdot\vec{r}} d^3k = |\delta_{\vec{k}}| e^{i\phi_{\vec{k}}}.$$

This means that when the Fourier transform is used the density pertubation can be expressed by a series of sine functions, each with the comoving wavenumber $\vec{k}$ and comoving wavelength $\lambda = 2\pi/k$. The power spectrum is given by (Ryden 2003):

$$P(k) = \langle |\delta_{\vec{k}}|^2 \rangle.$$

It expresses the mean square amplitude of the Fourier components, and the average is taken over all possible orientations of $\vec{k}$. Most theories of inflation predicts that the density fluctuations can be described by a Gaussian field characterized by the power spectrum,

$$P(k) \propto k^n$$

with $n = 1$. This is called the Harrison-Zel'dovich spectrum, and will be the form of the power spectrum right after inflation.

The shape of the power spectrum will however not stay the same, because gravity will cause the density perturbations to grow in amplitude. This is dependent on the nature of the dark matter i.e. whether hot or cold. Hot dark matter consists of particles that are relativistic at the time they decoupled from the rest of the Universe; in cold dark matter the particles were nonrelativistic. Hot dark matter has a large impact on the density perturbations, as the particles move freely in all directions with a relativistic velocity when the Universe is radiation-dominated, and thus smoothes out density perturbations that were present in the hot dark matter. This is called free streaming and removes all density perturbations smaller than the size of superclusters. Figure 1.2 shows the power spectrum of density fluctuations in both hot dark matter (once it has cooled enough to become nonrelativistic) and cold dark matter. It is seen that both the hot and cold dark matter follow the power spectrum of $P(k) \propto k$. However, the power spectrum for the hot dark matter falls sharply off and loses power at higher frequencies compared to the cold dark matter, as the density fluctuations have been removed by free streaming i.e. the fluctuations were too small. In the hot dark matter scenario the superclusters must have formed first, and clusters of galaxies and galaxies have then been formed afterwards from the superclusters. If most of the dark matter was cold, then the smallest structures would have formed first and afterwards the larger structures. This is also what we see from observations. The Universe is believed to have formed with the galaxies first and it also appears that the superclusters have just begun to form today (Ryden 2003).

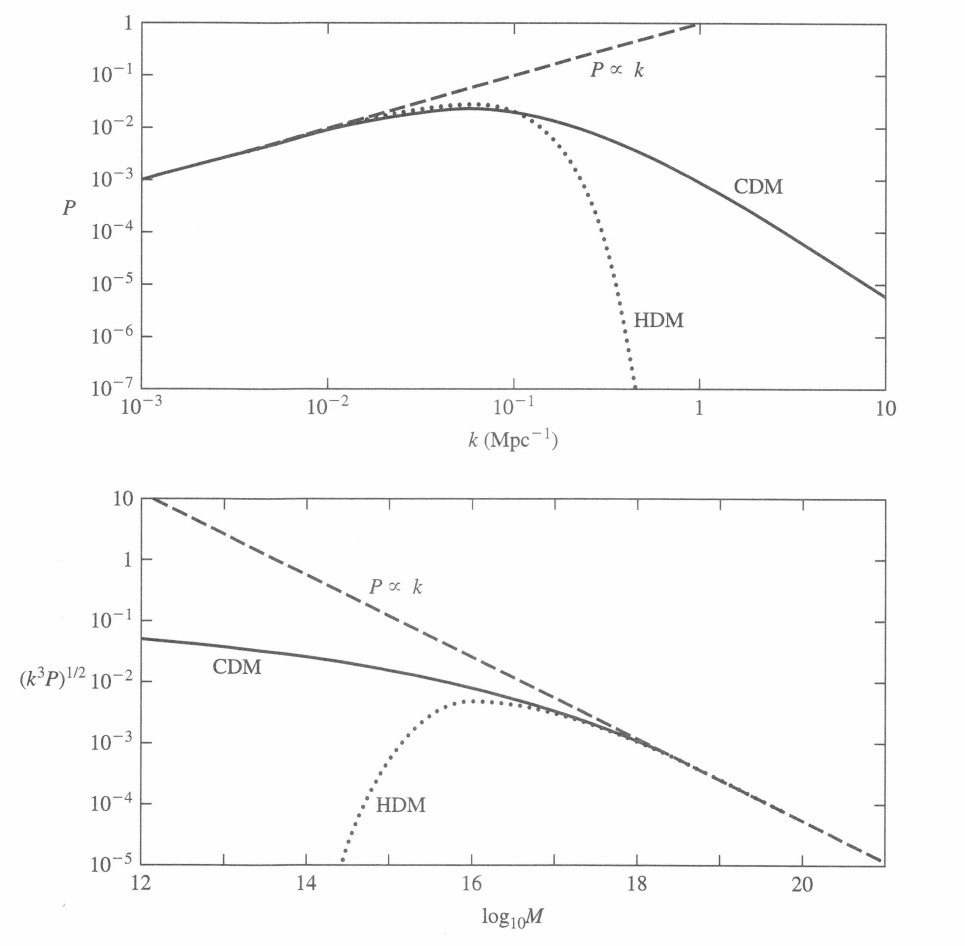

Figure 1.2: Upper panel: Power spectrum for cold dark matter (solid line), hot dark matter (dotted line) as well as the Harison-Zel'dovich spectrum. Lower panel: Root mean square of the mass fluctuations. For the hot dark matter the maximum amplitude occur at a mass scale of $M \sim 10^{16} M_{\odot}$ thus indicating that the first structures to form were the superclusters. For the cold dark matter the root mean square mass fluctuations have the largest amplitude at smaller masses thus implying that the smaller structures formed first (Ryden 2003).

1.2 Observing the High-z Universe

To understand the formation and evolution of structures in the Universe we need to determine the distribution of matter and large-scale structures. Thus we need to explore the early, i.e. the high-z Universe. Between $z \approx 0-6$ we have the optically observable Universe, where observations of quasars, Gamma Ray Bursts (GRB), and luminous galaxies have set a boundary for how far back in time we are able to see. This limit is gradually being pushed back as our technology improves. In the following sections I will describe the different types of probes for the high-z Universe.

1.2.1 Quasi-Stellar Objects

Quasars were discovered in the late 1950s when the first radio surveys of the sky were made. Most of the radio sources found were galaxies, but some of the radio sources looked like stars. Spectroscopic data from these star-like objects revealed strong and broad emission lines. In the 1960s it was realized from their emission lines that these objects were positioned at unprecedentedly large redshifts. They have luminosities in the range $10^{38} - 10^{42}$ W, i.e. they are a

thousand times more luminous than the Milky Way (Freedman & Kaufmann 2001). Because the physical nature of these star-like objects was unknown they were named 'quasars', which is short for quasi-stellar radio sources. They are a subclass of active galactive nuclei (AGNs) which are energetic phenomena in the central regions, or core, of galaxies.

It is believed that a black hole is the central engine that drives the quasars, since it is the only known engine that can provide the enormous energies that we see. The current model consists of a very massive black hole surrounded by an accretion disk. The energy is released when material gravitationally falls on to the disk and is heated. The radio properties of quasars can be categorized in two components, the extended (i.e. spatially resolved) and compact (i.e. unresolved at $1''$ resolution). The extended radio source usually has two almost symmetrical placed lobes of radio emission on either side of the optical quasar, i.e. perpendicular to the accretion disk. Besides this most quasars also have jets which connect the central source with the extended lobes, hereby transporting energy and particles out to the lobes. Jets are usually only seen on one side of the radio source. If a jet is seen on both sides, then one of the sides is much fainter than the other. This effect is caused by Doppler beaming which amplifies the surface brightness of the jet that approaches the observer (Peterson 1997).

Searching for radio sources were not the only way to find quasars. Another way was to search objects with an UV-excess, as the spectra of quasars show a higher ultraviolet flux compared to stars. Surveys of this type in the 1960s found a large population of quasar-like objects, but with ~ 100 times fainter radio emission. These radio-quiet objects were named quasi stellar objects or QSOs and they are the most numerous type as approx. 90% of the quasar population are radio-quiet QSOs. Today there is usually no distinction between the names quasar and QSO. However by some the term quasar is still used for radio-loud QSOs.

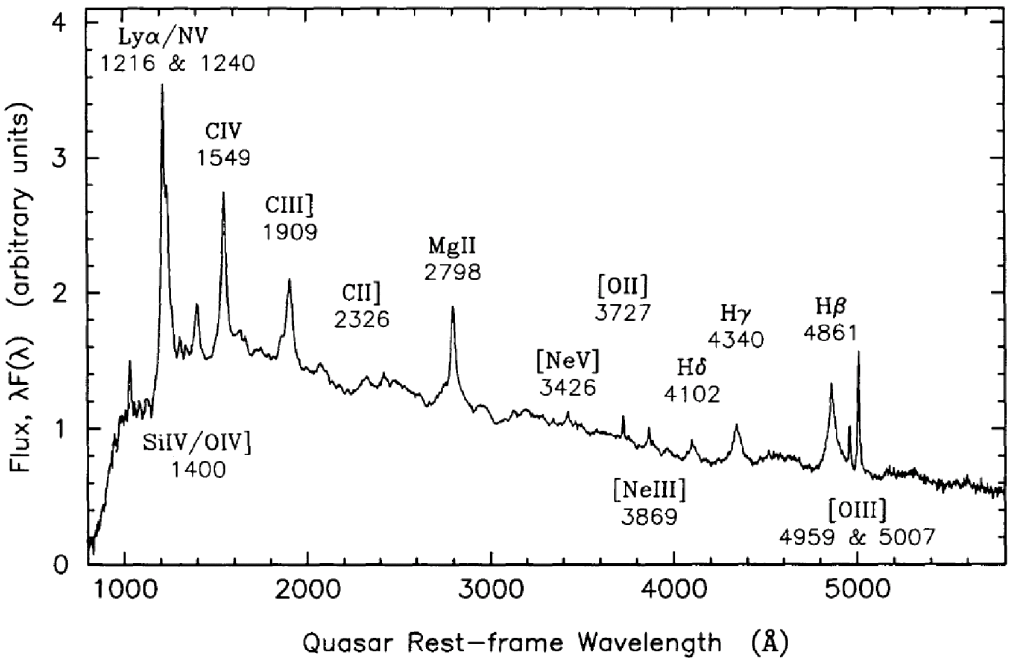

Figure 1.3: Composite quasar spectrum (Francis et al, 1991).

For almost all quasars the UV-optical spectra have been found to contain the strong emission lines of the hydrogen Balmer-series i.e. H$\alpha\lambda$6563, H$\beta\lambda$4861, and H$\gamma\lambda$4340. Other lines found

are Lyα as well as lines from abundant ions e.g. MgIIλ2798, CIII]λ1909, and CIVλ1549. The widths of the lines are different from object to object. Usually Doppler broadening causes the emission lines to blend. A composite spectrum averaged over several hundred QSOs is given in figure 1.3.

Because QSOs are so luminous their host galaxies are very hard to observe. However, absorption lines from the host galaxy can be found in their spectra at the same redshift as the emission lines of the QSO. One common result based on numerous imaging studies in the 1980s is that radio-quiet QSOs tend to be found in disk galaxies, whereas radio-loud quasars tend to be found in elliptical galaxies. It was also found that there is a correlation between the absolute magnitude of the host galaxy and the QSO or quasar such that brighter QSOs or quasars are located in more luminous galaxies. However, recent imaging observations with the HST has found that the correlation between the magnitude of the host galaxy and the QSOs was not as good as expected (Peterson 1997). This might be due to the fact that the host galaxy in several cases cannot be detected.

QSOs and Cosmology

As soon as the large redshift of the QSOs was discovered it became apparent that they were valuable in cosmology. Their high luminosities makes it possible to detect them at very large redshifts, hereby making them candidates for cosmological probes. The large redshifts enables us to study the Universe when galaxy formation is expected to have occurred. QSOs are found out to a redshift of $z \approx 6$, and with the Sloan Digital Sky Survey it should in principle be possible to detect QSOs out to $z \sim 6.5$ (Fan et al. 2001). This means that the light we recieve from them was emitted when the Universe were only about 6% of its present age. Detection of high redshift QSOs are important as they enable us to constrain the formation of large scale structures as well as follow the evolution of the Universe. Another aspect is that the QSOs will bring information on the formation of metals since these lines are seen in their spectra.

From very early on it was realized that the number of quasars per unit volume was not the same at all redshift. QSOs are very rare in the present-day Universe. Their density reaches a maximum at $z \approx 2$ - i.e. the era of QSOs were at a redshift of 2. Before this, the density of QSOs falls off sharply. This variation provides us with information regarding the evolution of galaxies and the Universe.

1.2.2 Absorption Systems

Already in the 1960s it was discovered that the spectra of QSOs often have absorption lines, usually at a redshift lower than the emission lines originating from the QSO. These lines are therefore caused by absorption from material that lies along the line of sight to the QSO. The absorption systems are either associated with the QSO or with physically unrelated objects, i.e. galaxies. QSOs can thus be used as tracers of the intervening material and hereby give information about the distribution of gas and structures in the Universe. Since QSOs can be found at large redshifts, the possibility of finding an absorber along the line of sight is non-negligible, and QSOs usually have several absorption systems.

The most commonly found absorption lines are Ly$\alpha\lambda$1216, MgII$\lambda\lambda$2796, 2803 and CIV$\lambda\lambda$1548, 1551. Besides these, the lines of CIIλ1335, SiIV$\lambda\lambda$1394, 1403 and MgIλ2852 are sometimes seen as well. In order to study the absorption lines of QSOs, high spectral resolution as well as a high signal-to-noise ratio are needed, since the lines are usually weak and unresolved. Whether a certain line is present in an observed spectrum depends on several factors. Firstly it depends

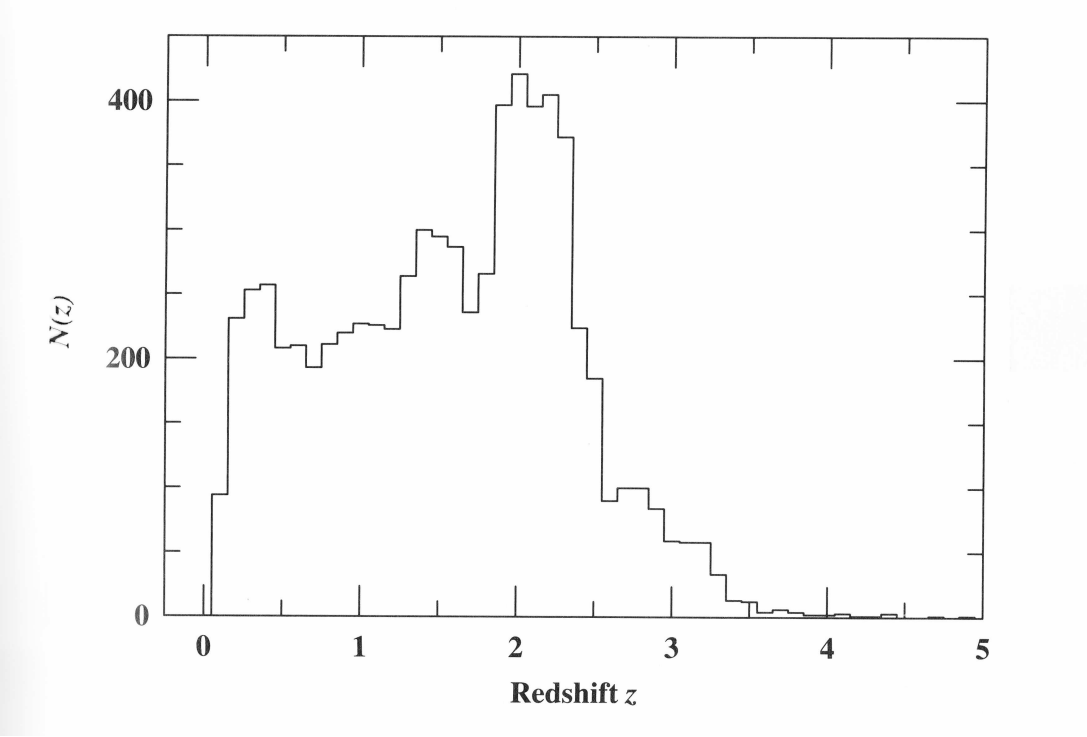

Figure 1.4: The quasar redshift distribution from the Hewitt and Burbridge (1993) catalog (Peterson 1997).

on the wavelength range of the observed spectrum, as the line might fall outside. The redshift of the QSO also have an impact as the larger the redshift of the QSO, the fainter the spectrum. The equivalent width of the absorption line depends on the spectral resolution as well as the signal-to-noise and this might put limitations to the observed lines as well.

There are several types of absorption systems for QSOs and I will briefly describe the most important aspects of these. However it is important to note that the absorbers are usually a combination of the described systems.

Lyα Forest Systems

The systems mentioned first are the Lyα systems. These occur when the light from the QSO with a wavelength of 1216 Å hits neutral hydrogen atoms and hereby boosting its electron to a higher energy state. Of course the more hydrogen atoms present, the larger the absorption. One way of selecting a type of absorber is by the means of the HI column density i.e. the amount of neutral hydrogen between the QSO and us. The content can be subdivided into three groups, where the Lyα forest systems have the lowest amount, corresponding to $N(\mathrm{HI}) < 10^{17}\mathrm{cm}^{-2}$ (Wolfe 2005). As numerous HI structures intervene along the sightline of the QSO, the spectrum is usually riddled with absorption features at wavelengths lower than the Lyα emission of the QSO itself. This is the Lyα forest where the column density of the absorbers is too low to produce detectable absorption lines except for Lyα. It is believed that the Lyα forest is caused by warm ionized hydrogen as this is optically thick in Lyα (Wolfe 2005). From simulations it is believed that there is a correlation between the local optical depth of Lyα and the dark matter density, thus making the Lyα forest a probe for the power spectrum of the dark matter as well as test the initial conditions of the Gaussian field (Weinberg et al. 2003).

Lyman Limit Systems

Lyman limit systems have HI column densities $10^{17}\mathrm{cm}^{-2} < \mathrm{N(HI)} < 2 \cdot 10^{20}\mathrm{cm}^{-2}$ and they show a sharp cutoff in the spectra of the QSO blueward of 912 Å in the rest frame of the absorber. This is caused by absorption of photons which are capable of ionizing HI. Lyman limit systems also show deuterium lines in their spectra and thus they might be used to determine D/H ratios and constrain the initial conditions for the primordial nucleosynthesis (Jedamzik & Fuller 1997).

Damped Lyα Systems

At column densities $N(\mathrm{HI}) \geq 2 \cdot 10^{20}\mathrm{cm}^{-2}$ the damped Lyα systems (DLAs) are formed (Wolfe 2005). The high column density of HI makes the damping wings of the Lyα absorption line optically thick hereby ensuring that the line is broad and strong. The equivalent width of these lines is usually ≥ 10 Å, making them easily distinguishable from other lines in the spectrum. The lines are so strong that they are easy to detect, and there is no need for the high spectral resolution required for other sorts of absorbers. Here the hydrogen is mostly neutral, and as stars form out of cold neutral gas that has clumped together to form molecular clouds, damped Lyα systems can be used as tracers of star formation at high redshifts. These absorbers are therefore believed mainly by Wolfe to be the disk of galaxies. Damped Lyα systems also contain a substantial amount of metals and can therefore be used to follow the chemical evolution of galaxies as well (Wolfe 2005).

Broad Lined Absorption Systems

The broad lined absorption systems have absorption features $\sim 10^4$ km s^{-1} wide on the shortward side of emission lines from abundant ions. This is an indication of absorbing gas flowing outward from the center of the QSO. The ionization level and outflow velocity are high, and it is therefore believed that these absorption systems are closely related to the QSO itself and they can thus be used to probe the regions close to the QSO. The lines seen in their spectra are usually from ionized species, e.g. CIV$\lambda\lambda$1548, 1551, SiIV$\lambda\lambda$1394, 1403, MgII$\lambda\lambda$2796,2803 and AlIIλ1671. The broad lined absorption systems are only seen for radio-quiet QSOs and are very rare; they only constitute about 12 % of the QSO population (Peterson 1997).

MgII Absorption Systems

Besides the previously mentioned absorption systems, the MgII systems are one of the important types. I will put emphasis on this type of absorption system as these are the key type of my thesis. Here the absorption system is selected on the basis of absorption of the resonance line doublet MgII$\lambda\lambda$2796, 2803. There are both strong MgII absorption systems with rest equivalent width of the lines of $W_r > 0.3$ Å, and weak systems with equivalent widths below this value.

The weak MgII absorbers trace HI gas and have hydrogen column densities below the Ly limit systems, i.e. $10^{16}\mathrm{cm}^{-2} < \mathrm{N(HI)} < 10^{17}\mathrm{cm}^{-2}$. They might either consist of one or several clouds i.e. show one or more MgII absorption lines. The weak MgII systems are believed to be due to supernova remnants or winds in dwarf galaxies or perhaps high velocity clouds (Lynch & Charlton 2007).

MgII absorption systems were among the first types of absorption systems discovered in the spectra of QSOs, since the MgII doublet have a large oscillator strength and the lines can be resolved fairly easily. In addition the rest wavelength of MgII makes it easy to detect even at larger redshifts. Usually the CIV absorption doublet lines are seen as well. The strong MgII systems mostly have hydrogen column densities $N(\mathrm{HI}) > 10^{17}\mathrm{cm}^{-2}$ and thus show Lyman limit or damped Lyα systems sometimes as well (Steidel 1995).

Most of the galaxies identified with MgII absorbers have an [OII]λ3727 emission line (Bergeron & Boisse 1991), which is also a sign of starforming regions, so one way of searching for potential galaxy counterparts of the absorbers is by means of the [OII] emission.

I will go into more detail about where the MgII systems are formed in section 1.4

1.2.3 Gamma Ray Bursts

In the 1960s a treaty was signed against nuclear testing and the US Air Force launched the Vela satellites to monitor if this treaty was violated by the USSR. As nuclear explosions emit large amounts of gamma rays, these satellites were sensitive to this sort of radiation and as a part of this military project flashes of gamma ray emission was found - coming from the sky and not the Earth. Hence the gamma ray bursts (GRB) were discovered. The first GRB was detected in 1967, but due to security reasons these data were not published until 1973 by Klebesadel, Strong & Olsen. A lot of theories were made as to whether the GRBs occurred close to earth e.g. in the Oort cloud, in the Milky Way, or at cosmological distances (Nemiroff 1994). The theories connecting the GRBs with galactic distances were favoured in the beginning due to the fact that the high energy output from the GRBs could then be explained more easily.

In 1990 the Compton Gamma Ray Observatory (CGRO) was launched, and one of the instruments onboard was the Burst And Transient Source Experiment (BATSE) which could monitor nearly the whole sky and detect as well as locate the transients of GRBs, which outshine everything else in the gamma-ray sky. With BATSE it was possible to determine the distribution of GRBs, and this is displayed in figure 1.7.

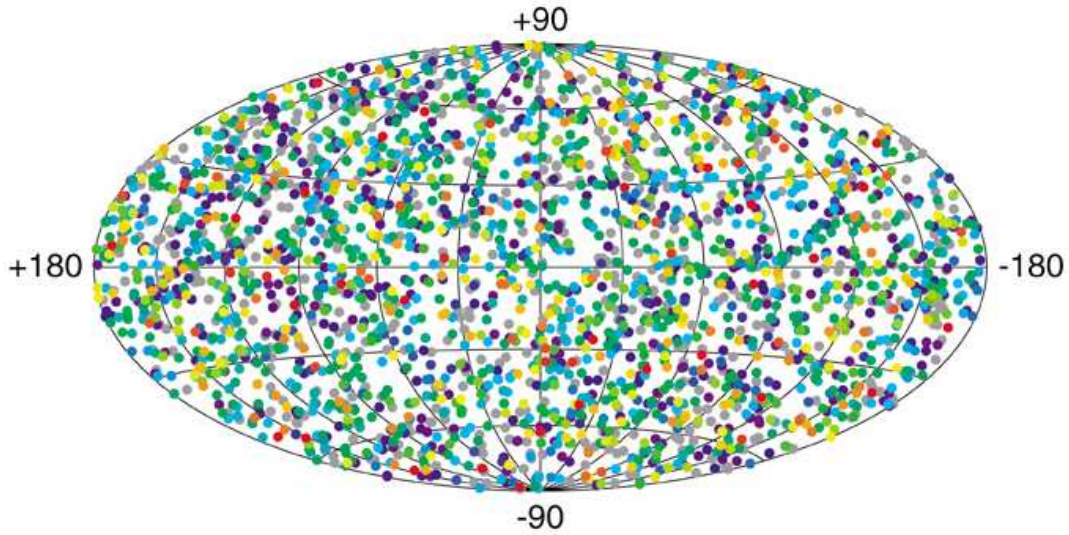

Figure 1.5: The distribution of GRBs obtained by BATSE (http://cossc.gsfc.nasa.gov/docs/cgro/batse/).

As is seen, the GRBs are located uniformly across the sky and there is approximately one GRB per day. The theory connecting the GRBs to the Milky Way was thus ruled out, since the GRBs are not concentrated to the plane of the Galaxy. However, since distances cannot be measured from the Gamma Ray emission, it was still not known if the GRBs had extragalactic origin.

Afterglow

The clue to whether the GRBs had extragalactic origin came with the Italian X-ray satellite BeppoSAX. This satellite revolutionized the GRB astronomy as it was able to quickly (within hours) pinpoint a GRB position with an error circle of a few arcminutes. On February 28, 1997, a GRB was detected by BeppoSAX and already after ∼20 hours the ground based William Herschel Telescope on La Palma was used to gather optical observations. When compared to observations made a week later an object was found that did not appear on the second observation and hence the first optical transient was found. The BeppoSAX satellite also discovered an x-ray afterglow approx. 8 hours after the burst that faded gradually and eventually disappeared. It had a position which was consistent with the location of the optical afterglow of the GRB. After the optical afterglow faded away, a faint galaxy was discovered very close to the position of the GRB which might be a possible host galaxy.

The GRB afterglows appear after the gamma-ray radiation disappears and usually last for days to months, getting weaker with time and evolving from x-rays into less energetic radiation such as visible light and eventually radio radiation. It is believed that the afterglow is characterized by electrons moving in a magnetic field with velocities close to the speed of light (Gehrels, Piro & Leonard 2002).

Another breakthrough came with the detection of the GRB970508. For the first time the redshift of a GRB was measured on the basis of the afterglow and the result was $z = 0.835$ (Metzger et. al. 1997, http://www.cfa.harvard.edu/iauc/06600/06676.html#Item3). This proved that the GRBs are extragalactic and the highest redshift measured so far is for the GRB050904 with $z = 6.3$ (Campana et. al. 2007). Thus the bursts must be very energetic and usually energies higher than 10^{52} ergs are released. Beaming might also have an impact on the observed energy output. If the burst would beam its energy in some narrow angle instead of in all directions, the observed luminosity would be lower. This might be what caused the afterglow of GRB990123 to dim rapidly two days after the burst (Gehrels, Piro & Leonard 2002). This is due to the fact that when the jet moves close to the speed of light, it emits light in narrow beams that bypass the observer. As the jet slows down these beams gets wider and eventually the jets comes into view. Eventually there is nothing left to be seen and the apparent brightness falls off rapidly. We will only see the GRB if the jet is along our line of sight. Usually the beam size is a few degrees (Gehrels, Piro & Leonard 2002).

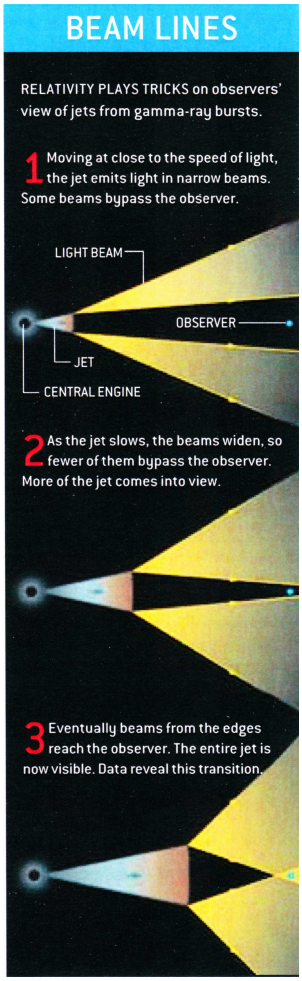

Figure 1.6: Beaming effect (Gehrels 2002).

Progenitors

How are GRBs formed and what produces their afterglow? The prompt gamma ray emission roughly divides the GRBs into two classes depending on the duration of the burst, typically lasting between a few milliseconds up to several minutes. Most GRBs are long-soft bursts which have a duration longer than two seconds. The other class is the short-hard bursts which have a duration less than two seconds. These bursts also have a harder spectrum, i.e. they emit more high energy gamma rays, and they do not have an afterglow compared to the long-soft GRBs.

This also implies that there are two different mechanism creating the long and short GRBs. Since the long-soft GRBs have afterglows it has been easier to establish a theory for this type of GRB. There seems to be some diversity in the population of long duration GRBs and this is especially seen in the structure of their lightcurves. They do not have the same duration and luminosity and some might have more than one burst. This suggests that the progenitors might be different. Based on the shape of some GRB lightcurves, it has been proposed that most of the long duration bursts are linked to supernovae Ib/c or hypernovae (Nomoto et al. 2007; Woosley & Bloom 2006). However, this is still debated (Fynbo et al. 2006 & Watson et al. 2007). Iron has also been found in the x-ray spectra of several bursts, which is seen in supernova explosions as well.

Due to the high energy of the GRBs it was very early realized that they are most likely caused by the gravitational collapse of a massive star into a neutron star or a black hole. The general idea of a progenitor is that the core rotates rapidly before the collapse and some of the infalling material creates a torus around the compact object, in most cases believed to be a black hole. Thus the system is energetically fuelled by the rotational energy of the black hole and gravitational energy of the disk. In order to achieve a high enough rotation to form a torus, the progenitor is believed to be either a massive metal-poor star and/or perhaps a tight binary system where the primary is a black hole which can tidally spin up the core of the secondary, hereby producing the GRB (Davies et al. 2007). The masses of the progenitors are believed to be $> 20 M_{\odot}$ (Davies et. al. 2007) in order to generate the energies needed.

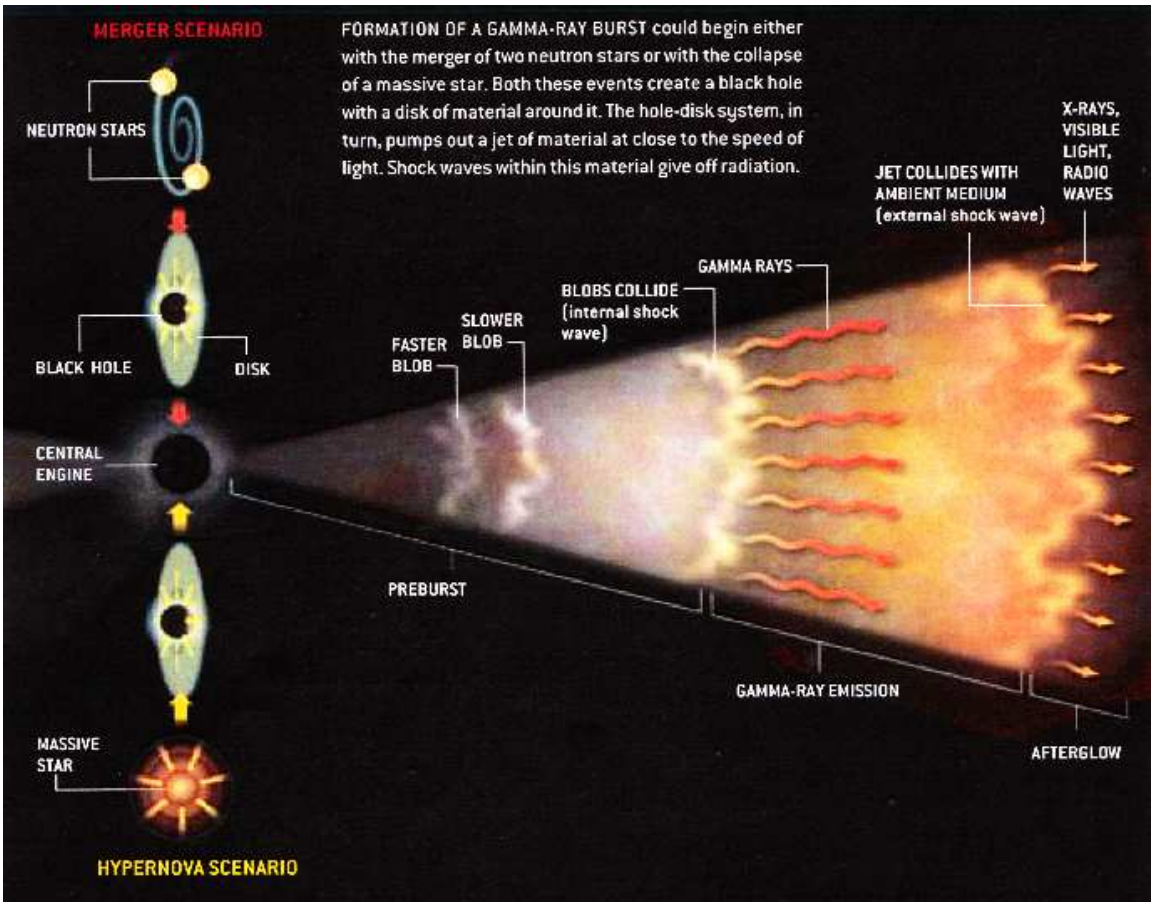

Figure 1.7: Fireball Model (Gehrels 2002).

It is believed that an intense magnetic field is built up during the formation of the disk and causes it to be heated up to such high temperatures that a great fireball of gamma rays and plasma is created and moves away in narrow jets along the rotation axis with velocities at almost the speed of light. The gamma-rays are caused by internal shock waves formed when faster moving blobs of plasma collide with slower ones. This so-called fireball theory can also explain how the afterglows are formed. This happens when the expanding fireball collides with surrounding gas of the external medium and creates another shock wave as the fireball slows down hereby emitting x-rays, visible light and in the end radio waves (Gehrels 2002).

Long duration GRBs seem to be connected to star forming regions in the host galaxies and thus it has been suggested that the progenitor of long duration bursts are Wolf-Rayet (WR) stars (Chevalier 2007, Marle, Langer & Garcia-Segura 2007, and Woosley 1993). WR stars have masses higher than $20M_{\odot}$ and they have strong winds, hereby expelling large amounts of heated gas. This material thus embeds the WR star and might be seen in the spectra of GRBs as an absorption system in the GRB environment. As the massive stars leading to hypernovae have a short lifetime, they are also expected to occur in star forming regions, and thus it is believed that long duration GRBs are connected to the hypernovae scenario. As for the binary model the evolution is much longer (up to billions of years) and is not connected to star forming regions. This model might explain the short-hard duration GRBs (Gehrels 2002).

GRB sightlines and MgII absorption systems

Along the sightlines of GRBs the same types of absorption systems are found as for QSOs e.g. damped Lyα systems and Lyman limit systems. Apart from the absorption features, GRB afterglows are usually featureless, making it easier to identify the lines. However one intriguing aspect is in the connection of intervening MgII absorbers. GRB afterglows fade away and leaves a clear sightline for deep imaging observations. This can be used in the search for galaxy counterparts of MgII absorbers and I will explain this in section 1.4. Firstly I would like to give a short introduction to absorption physics and statistics.

1.3 Absorption Physics

In this section I would like to give a short review of some of the physics behind absorption lines as well as the statistical analysis of the number of absorbers along the line of sight to a background source e.g. a GRB or a QSO. As it is known that the absorbers are most probably connected to galaxies, I will also elaborate on what can be said about them.

1.3.1 Absorption-line Physics

Absorption lines are seen as a dip in the continuum light of a spectrum and can be represented by the equivalent width (Emerson 1997):

$$W(\lambda_0) = \int_0^{\infty} \frac{F_c(\lambda) - F_l(\lambda)}{F_c(\lambda)} d\lambda = \int_0^{\infty} (1 - e^{-\tau(\lambda)}) d\lambda,$$

where F_c is the flux of a neighbouring continuum point and F_l is the flux in the absorption line, both at wavelength λ. Since it is an absorption line, the flux in the line is less than in the continuum and hence the equivalent width is always positive. The optical depth, τ, of the absorbing material is given by:

$$\tau(\lambda) = \int n(l)\sigma(\lambda) dl = N\sigma(\lambda).$$

Here N is the column density defined by the integral of the particle density in the lower state, $n(l)$, integrated over the path length, l, i.e. $N = \int n(l)dl$. σ is the absorption cross section (Peterson 1997). The width of the line also depends on natural broadening. This is caused by Heisenberg's uncertainty principle, which means there will be an uncertainty in the spread of the energy level yielding a broadened line. Natural broadening will always be present. Apart from this Doppler broadening, i.e. broadening caused by motions of the particles in the absorbing gas, is present as well. The strength of an absorption line at a certain wavelegth can be parameterized by the integrated strength over all wavelengths, i.e.:

$$\int \sigma(\lambda)d\lambda = \frac{\pi e^2}{m_e c}\frac{f\lambda_0^2}{c} = \frac{\lambda_0^4}{8\pi c}\frac{g_2}{g_1}A_{21}.$$

f is the oscillator strength of the line, g_1 and g_2 are the statistical weights of the lower and upper levels, and A_{21} is the Einstein coefficient for the transition (Peterson 1997).

To estimate how many absorption systems we can expect along a given sightline, we need to use statistics. First we need to consider the number of absorption lines that might be seen. This is given by:

$$dN(z) = n(z)\sigma(z)dr_{proper}(z).$$

Here n is the number density of absorbers, σ is the absorption cross-section, and dr_{proper} is the proper length. In order to determine the proper length we also needed to use the Robertson-Walker metric describing the geometry of the Universe (Ryden 2003):

$$ds^2 = -c^2dt^2 + a(t)^2[dr^2 + S_k(r)^2(d\theta + \sin^2\theta d\phi^2)],$$

where $a(t)$ is the scale factor, normalized to 1 at the present epoch, and r is the comoving coordinate. $S_k(r)$ is a distance measure for the three different types of curvature (Ryden 2003):

$$S_k(r) = \begin{cases} R\sin(r/R) & \text{for } k = +1 \\ r & \text{for } k = 0 \\ R\sinh(r/R) & \text{for } k = -1 \end{cases}.$$

k is the curvature constant, where $k = +1$ for a positively curved space, $k = 0$ for a flat space, and $k = -1$ for a negatively curved space. For a curved space, R is the radius of curvature.

Usually it is assumed that both the cross-section of the absorbers and the comoving space density are constant so that $n(z) = n_0(1+z)^3$. This implies that (Fynbo 2000):

$$\begin{aligned} \frac{dN(z)}{dz} &= n_0(1+z)^3\sigma_0\frac{dr_{proper}}{dz} \\ &= n_0(1+z)^2\sigma_0\frac{dr}{dz} \\ &= \frac{\sigma_0 n_0(1+z)^2}{\sqrt{(1+z)^2(\Omega_0 z+1) - \Omega_\Lambda z(z+2)}}, \end{aligned} \tag{1.1}$$

where the density parameters, Ω_0 and Ω_Λ are given by the critical density, ρ_0, and the cosmological constant, Λ (Ryden 2003):

$$\Omega_0 = \frac{8\pi\rho_0 G c^2}{3H_0^2} \quad \text{and} \quad \Omega_\Lambda = \frac{\Lambda c^2}{3H_0^2}.$$

From eq. 1.1 it is seen that when $\Omega_\Lambda = 0$ and $\Omega_m = 1$, dN/dz is a power-law in (1+z) and thus the evolution of the number density is commonly parameterized as:

$$\frac{dN(z)}{dz} = \left(\frac{dN}{dz}\right)_0 (1+z)^\gamma. \tag{1.2}$$

This means that for $\gamma > 1$ there would be evolution, and thus either the comoving density or the cross-section is larger at higher z. Normally the average number of absorbers in a survey, $\overline{N(\langle z \rangle)}$, as well as the redshift interval, δz, are used as an approximation:

$$\frac{dN(z)}{dz} \approx \frac{\overline{N(\langle z \rangle)}}{\delta z},$$

and thus by fitting these data to eq. 1.2 an estimate can be found for $(dN/dz)_0$ and γ. It has been found that the strong MgII systems for QSOs are evolving, with $\gamma = 2.47 \pm 0.68$ and $(dN/dz)_0 = 1.19$ (Peterson 1997).

Since research shows that MgII absorption systems are connected to galaxies and trace HI as well, the galaxy luminosity function, Φ, can be used to determine the number of intervening galaxies, i.e. absorbers. This can be expressed by (Wolfe et al. 1986):

$$\frac{dN}{dz} = \left(\frac{c}{H_0}\right) \frac{(1+z)}{(1+2q_0 z)^{1/2}} \int_0^\infty dL \Phi(L) A(L),$$

where $A(L)$ is the average cross section of the intervening galaxy with luminosity L. To express this variable two relations are usually used, i.e. the Holmberg relation and the Bosma relation. The Holmberg relation is the scaling relation (Peterson 1997):

$$R(L) = R_* \left(\frac{L}{L_*}\right)^t.$$

R_* is the radius of a galaxy with luminosity L_*. The Holmberg radius R_H is defined to be the radius of the isophote with a surface brightness of 26.5 mag arcsec^{-2} in B. For $L = L_*$ the corresponding radius is the Holmberg radius $R_* = R_H$. Wolfe et al. (1986) found a way of describing the number density for damped Lyα systems. Here the Bosma relation is used to describe $A(L)$ and this states a relation between the Holmberg radius and the radius of HI, i.e. $R_{LIM}/R_H = \xi$ (Wolfe et al. 1986). By using these two relations, the expression for the cross section is normally written (Wolfe et al. 1986):

$$A(L/L_*) = (\pi R_*^2/2)(L/L_*)^{2t} \xi^2.$$

The galaxy luminosity function is a so-called Schecter function (Peterson 1997):

$$\Phi(L)dL = \Phi_* \left(\frac{L}{L_*}\right)^{-s} \exp\left(-\frac{L}{L_*}\right) d\left(\frac{L}{L_*}\right)$$

and when combining these a general expression for the number density of absorbers is obtained (Wolfe et al. 1986):

$$\frac{dN}{dz} = K \frac{(1+z)}{(1+2q_0 z)^{1/2}},$$

where

$$K \propto (\xi R_*)^2 \Phi \Gamma(1+2t-s) \qquad \text{and} \qquad \Gamma(\mathrm{x}) = \int_0^\infty \mathrm{t}^{\mathrm{x}-1} \mathrm{e}^{-\mathrm{u}} \mathrm{du}.$$

These equations make it possible to give an approximation for how the number of absorbers varies with the redshift. They are for damped Lyα systems, but the same can be done for other types of absorbers.

1.4 MgII Absorption Systems

It is not yet known exactly where in a galaxy the MgII absorption is formed. It is known to be a tracer of cold gas, but in which part of the galaxy is still up to debate, and several theories exist.

One theory is that the absorption is caused by supernova outflows or superwinds in the halo of the host galaxy, and this scenario might also explain the absorption in the vicinity of the QSO. Here the absorption selected galaxies trace the colder and denser gas of the outflow (Bouché et. al. 2007). In several studies it has been found that absorption selected galaxies at higher redshifts (i.e. $z > 1$) have relatively high star formation rates and are thus possibly related to starburst galaxies, especially for the strongest MgII absorbers where the hosts are generally bluer (Bouché et al. 2007). Large starbursts might also create more supernova outflows and hereby support that theory. Bouche et. al. (2007) finds, on the basis of detection of Hα emission and high star formation rates with SINFONI observations of a MgII selected sample, that the outflow scenario is a possible explanation for strong MgII absorption ($W_r > 2$ Å). The strong MgII absorbers might also be connected to Lyman break galaxies, which are also thought to contain starburst regions (Adelberger et al. 2003).

One of the persistent theories concerns the large extended gaseous halos around luminous galaxies. This model associates the MgII absorption with the gaseous halo in a two-phase structure. One is a shock-heated hot phase where photoionized clouds moves through the halo. In this model the MgII systems are thought to arise in the halo of relatively massive galaxies, where the gas is dense enough to radiate the energy from the shock-heated gas (Prochter, Prochaska & Burles 2006). Observations also show that strong MgII absorbers out to $z \simeq 1$ are believed to be associated with $\sim 0.7L_B^*$ late time Sb galaxies i.e. luminous spiral galaxies (Steidel et. al. 1994) with impact parameters between 5" and 12" or the linear distance 1.5 to 3.5 R_H where $R_H = 22$ kpc with $H_0 = 50\text{km s}^{-1}\text{ Mpc}^{-1}$ (Bergeron & Boissé 1991).

At larger redshifts the absorbers are possibly connected to the gas in halos of luminous galaxies, but starforming faint blue galaxies seem to have an impact as well as they might be gravitationally bound to the luminous galaxies (Steidel 1995).

One way to elucidate the physical nature of strong MgII systems is to look at their incidence as a function of cosmological time, i.e. dN/dz (see eq.1.2). Since the number density as a function of redshift is very sensistive to mass, this might be the means of figuring out what the masses of the halos are. Prochter, Prochaska & Burles (2006) performed an estimate of the number density as a function of redshift for strong MgII absorbers (with $W_r > 1.0$ Å) for SDSS data. Figure 1.8 shows this incidence in the redshift range $z = 0.35 - 2.3$ where the green triangles show the whole dataset, the red squares show systems with $1.0\text{Å} < \text{W}_\text{r} < 1.4\text{Å}$ and the blue cross-hatches show the systems with $W_r > 1.8$Å. It is seen that the samples show similar evolution. At $z > 0.8$ the slopes of the curves are nearly constant and at $z < 0.8$ there is a decrease in dN/dz. These data cannot be fitted by the simple power law as this fails to describe both the increase in dN/dz at low redshifts and an almost constant value for larger z. Prochter, Prochaska & Burles (2006) used cuts in the data to perform the fits and obtained an incidence rate of $dN/dz = 0.174 \pm 0.002$ in the redshift region $0.35 < z < 2.3$. Since the number density evolution of the MgII sample is fairly constant over a fairly large redshift sample Prochter, Prochaska & Burles argue that the cross section of the MgII systems are very likely connected to dark matter halos with masses $10^{11} - 10^{12} M_\odot$.

Even though some possible absorption systems have been found close to or at the absorption

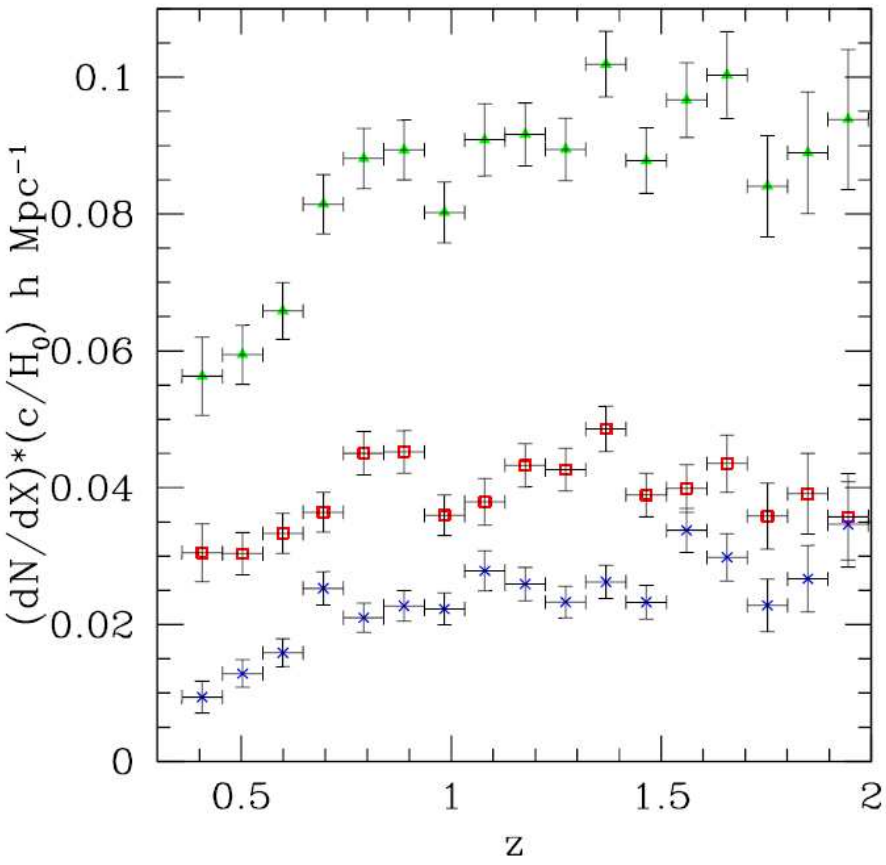

Figure 1.8: The incidence of strong MgII absorbers. The green triangles show the whole dataset, the red squares show systems with 1.0Å < W_r < 1.4Å and the blue cross-hatches show the systems with W_r > 1.8Å (Prochter, Prochaska & Burles (2006)).

redshift, at a somewhat high impact parameter, there has always been doubt as to whether the found object is in fact the absorber. This is because the true absorbers might be faint galaxies that lie at small impact parameters and thus are hidden inside the bright glare of the QSO.

GRBs provide an unique probe on this issue since their afterglows fade away, leaving a clear sightline, where deep imaging can be used to search for possible faint absorbers. Research already shows that such faint absorbers might have gone undetected. A search for the MgII absorption systems for GRB021004 carried out by Vreeswijk, Møller & Fynbo (2003) showed that no galaxies brighter than 0.1 L* were found within 10" of the GRB, so there is the possibility that the galaxies are much fainter. The large galaxies might also just be the brightest neighbours to dwarf galaxies that are the actual absorbers. For Damped Lyα systems at high redshifts, the impact parameters are usually found to be at the order of 10 kpc, and not 100 kpc as is expected for the large luminous galaxies (Møller et al. 2002a). Furthermore, Jakobsson et al. (2004) found an absorber at an impact parameter of 1."2 for GRB030429, which could mean that previously found galaxies at large impact parameters might not be the actual absorbers. This is the precise topic of my thesis, as I am searching for these faint galaxies at small impact parameter to the GRB.

1.5 GRB vs. QSO sightlines

Recent studies by Prochter et al. (2006) has found a higher incidence of strong MgII absorbers along the sightlines of long duration GRBs compared to QSO sightlines. Their sample consisted of 14 GRBs and among these 14 intervening strong ($W_r > 1$) MgII absorbers were found (i.e. some of the sightlines had several intervening absorbers and others had none), based on the selection criterion that both members of the MgII doublet should be detected above a 3σ significance. The number of GRB sightlines that can be used for a MgII search is represented by the redshift path density $g(z)$ (see top panel in figure 1.9). To illustrate the difference between GRB and QSO sightlines, the redshift path density was convolved with the observed incidence of MgII systems per unit redshift. This is displayed in the bottom panel of figure 1.9 where the cumulative number of MgII absorption systems detected along GRB sightlines (black line) is shown as well as the prediction based on statistics for QSOs (grey line). The QSO statistics were based on over 50,000 quasars with 7000 strong MgII absorbers from the SDSS survey.

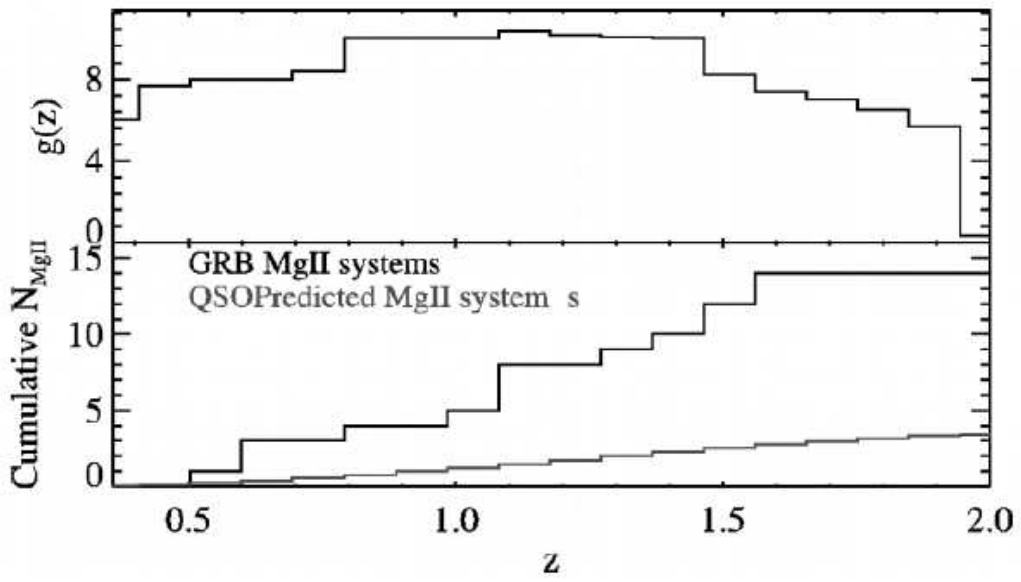

Figure 1.9: Upper panel: The redshift path density. Lower panel: The cumulative number of MgII absorption systems (black curve) and the prediction based on statistics (grey curve) (Prochter et al. 2006).

The figure shows that there is a significantly higher abundance of MgII absorbers along GRB sightlines. It has been estimated that there are an approx. four times higher incidence of MgII absorbers along GRB sightlines, which cannot be due to statistical fluctuations (Prochter et al. 2006).

Several theories have been proposed to explain this difference. One theory is dust obscuration bias, where dust in the MgII absorbers could obscure the optical light from faint QSOs and hereby lead to an underestimate of the incidence of MgII systems per unit redshift for the QSOs. Radio-selected QSOs are not affected by dust, but they only represent a small sample of the whole QSO population. Porciani, Viel and Lilly (2007) find that the incidence rate of MgII systems could be underestimated by a factor of 1.3-2 due to dust obscuration, but this does not explain the whole difference that is seen.

Frank et al. (2006) suggested that the beam sizes of GRBs and QSOs as well as clumpy intervening MgII absorbers might be the cause of the observed difference, i.e. they propose a

geometrical solution where the beam size of QSOs are approx. two times larger than for GRBs and the size of the MgII absorber is comparable to the beam size of the GRB. This would lead to lower equivalent widths along QSOs sightlines. As pointed out by Prochter et al. (2007) and Pociani, Viel and Lilly (2007) this theory does not hold as there have not been observed any unsaturated MgII lines where the doublet ratio is not 2:1. If the saturated systems should have been diluted by a larger QSO beam the MgII doublet ratio would be 1:1.

Another possible scenario is that since the strong MgII absorbers are possibly located in dark matter halos with masses of $10^{11} - 10^{12}$ $M_{\odot}$ (Bouche et al. 2004), the background GRBs could be gravitationally lensed. This would lead to a selection bias towards bright optical afterglows. Furthermore, nearly every GRB sightline has a MgII absorption system and afterglows with more than one MgII absorber have been found to be on average 1.7 times brighter than others (Porciani, Viel and Lilly 2007). However there are also several arguments against this theory. The very bright afterglows that are seen cannot be readily explained by galaxy or cluster lensing alone, and there have not been observed any multiple images as is usually seen in connection with lensing, nor any bright foreground galaxy (Prochter et al. 2007). Moreover, it is also believed that the MgII absorption systems are located at large impact parameters, which goes against the lensing theory. I am, however, searching for small impact parameter systems and might find a different result, hereby eliminating the impact parameter argument against the lensing theory.

As the discrepancy has been found for MgII systems, similar studies have been carried out for CIV absorbers. Contrary to MgII absorbers, no difference is seen between the incidence of CIV absorbers along the sightlines to GRBs as opposed to QSO sightlines (Sudilovsky et al. 2007; Tejos et al. 2007). However, the CIV systems are usually found at larger impact parameters, they have less dust extinction, higher redshift, and a larger number density dn/dz compared to MgII systems, and they also contain more ionized gas than MgII systems. Thus the two types of samples cannot be used for direct comparison, but statistically they might constrain e.g. the dust content, mass and column densities of the galaxies hosting the metal absorbers.

No clear explanation for the higher incidence of MgII absorbers along GRB sightlines has been found yet. It is possible that several of the proposed theories might contribute and it is still a research area of great debate.

Chapter 2

Selection of Target Fields

An important aspect of most observational Astrophysics is how the targets are selected. In this chapter I will therefore describe the selection process and the chosen target fields for my work.

2.1 Selection process

The goal of the observations is to do a systematic search for the galaxies that are responsible for MgII absorption along the line of sight to GRBs. The main problem is the magnitude limit and the possibility that the absorbers might be below the detection limit and thus will not be found. The idea is therefore to compare with previous work by probing down to comparable luminosities ($L \sim 0.1L^*$), but at much smaller impact parameters. This way will make it possible to find out whether faint galaxies at small impact parameters (< 5") might have been previously overlooked.

The GRB field sample was selected based on the MgII detection in the afterglows. For all of the GRBs there exist a good spectrum of the afterglow. The criterion is that the MgII absorption must have been detectable in the afterglow at a resolution of $R > 500$ and a $S/N > 15$.

For my thesis, the three GRB target fields of GRB021004, GRB030226 and GRB020813 have been selected. The number of fields was limited by the amount of time available for a master's thesis.

2.2 Target fields

2.2.1 GRB021004

GRB021004 is one of the brightest afterglows detected. The burst was detected by the *HETE-2* satellite at the position RA. 00:26:54.69 and Decl. +18:55:41.3 (J2000) (Fox 2003). Already 10 min after the burst the optical afterglow was discovered at R = 15.3 (Fox 2002, Fox 2003). Due to the very fast discovery of the optical afterglow it was possible to get a good sampling of its light curve. Early on two absorption systems were found with absorption lines of MgI, MgII and FeII (Fox 2002, Fox 2003), and the redshift was later confirmed by e.g. Møller et al. (2002) to be at z = 1.3806 and z = 1.6039. An emission line from Lyα at z = 2.3351 from the host galaxy was also seen in the spectra (Møller et al. 2002). AlII absorption was found at the same redshift as well, which confirms the redshift of the host galaxy. The host galaxy is relatively blue with the magnitudes R=23.95±0.08 and B=24.60±0.06 (Fynbo et al. 2005; Mirabal et al. 2003). It is an active starburst galaxy with a SFR of 15 $M_\odot$ yr^{-1} (Djorgovski et al. 2002), which is above the average rate at that redshift. Besides this, several absorption lines were found with a velocity distance up to 3000 km s^{-1}. This might be due to the absorbing material being a fragmented shell nebula located around the GRB site (Mirabal et al. 2003), a clumpy wind expelled by

a massive progenitor, or perhaps by the GRB exploding within a clumpy supernova remnant (Lazatti et al. 2002). The afterglow spectrum also showed deviations from the usual power-law decay with bright bumps, possibly caused by the fireball interacting with dense clumps in the sorrounding medium (Lazatti et al. 2002).

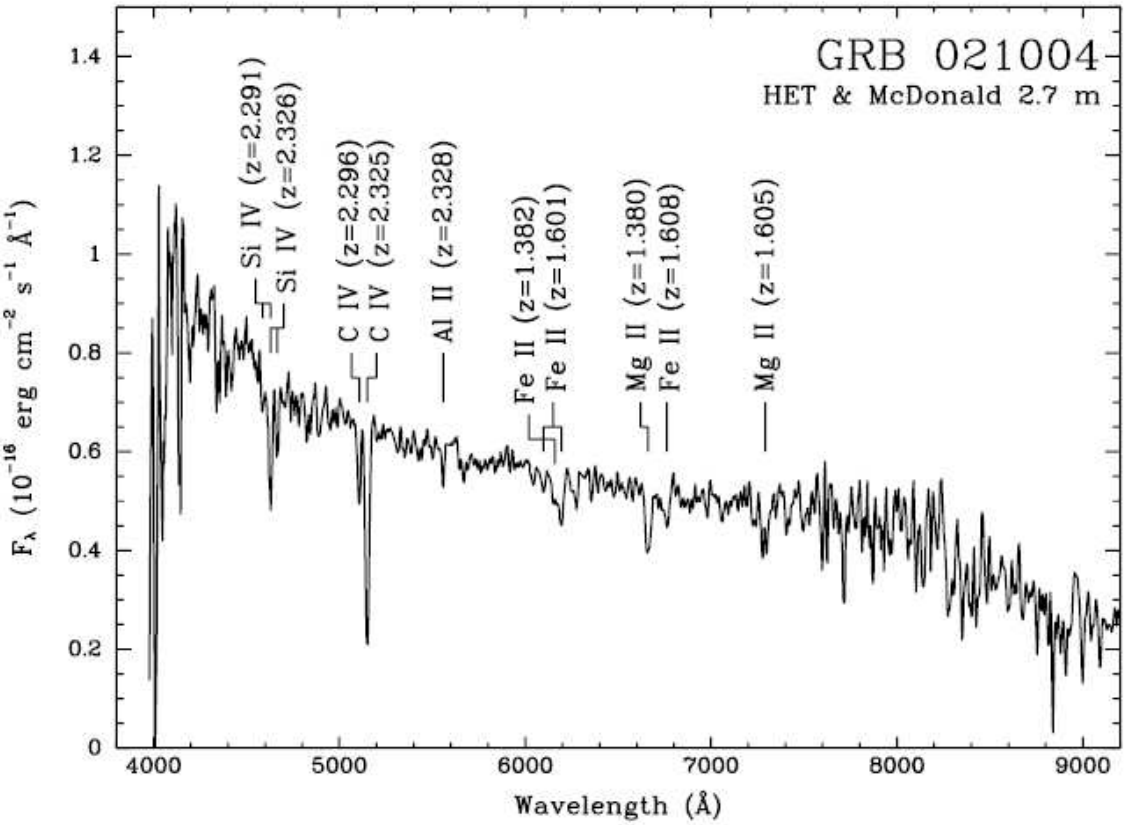

Figure 2.1: Combined spectrum of GRB021004, where the absorption systems are shown. Longward of 5800 Å the intervening MgII systems are seen. The other absorption systems are formed in the environment of the GRB (Schaefer et al. 2003).

Absorption systems

Five absorption systems have been found in the afterglow spectrum at redshifts 1.3806, 1.6039, 2.2983, 2.3230, 2.3292 (Møller et al. 2002b). The two systems at the lowest redshift are intervening absorbers. The system at z=2.3292 is at a velocity distance of 530 km s^{-1} from the host galaxy at z=2.3351 determined from Lyα emission. The absorption system at z = 2.2983 is at a velocity distance of 3300 km s^{-1}. Thus the three absorption systems are blueshifted relative to the host galaxy Lyα emission. For DLAs and Lyman-Break galaxies a velocity shift is normally seen between the redshift of the Lyα emission and Lyα absorption (Møller et al. 2002a; Adelberger et al. 2003). This shift is possibly caused by absorbing gas in a galactic wind moving towards us. This will make the absorber blueshifted, and the resonantly scattered Lyα photons will try to escape the cloud and hereby also get redshifted. However, the large shift of 3300 km s^{-1} seen here has not been observed in Lyman-Break galaxies, and it should only be of the order of 200 km s^{-1} or less. This means that the three absorbers at the highest redshift must be in the local environment of the GRB, as these large shifts cannot be due to the normal properties of the host galaxy (Møller et al. 2002b).

Table 2.1: Absorption features in GRB021004 (Fiore et al. 200)

Ion	λ_{obs} (Å)	W_r (Å)	z_{abs}
MgIIλ2796.35	6657.70	0.47 ± 0.02	1.3807
	7278.39	0.24 ± 0.01	1.6028
MgIIλ2803.53	6674.77	0.32 ± 0.02	1.3807
	7296.85	0.23 ± 0.01	1.6028

One possible explanation for the absorption systems closest to the GRB could be that the GRB progenitor was a Wolf-Rayet star which lost its outer envelope by a stellar wind. The wind could then have reacted with the neighbouring ISM, creating shocks. This would lead to the formation of overdense shells or shell nebulae (Mirabel et al. 2003; Schaefer et al. 2003). Marston (1997) also found that approx. 35% of all Wolf-Rayet stars have shell nebulae. Radiative acceleration of the shell nebulae by the GRB afterglow would create velocity structures of the blueshifted absorbers and could also lead to "line locking", which has been proposed by many (i.e. Møller et al. 2002b; Savaglio et al. 2002). The absorbers in GRB021004 show similarity to the ejected systems of QSOs. As for QSOs, they have strong absorption of highly ionized CIV and SiIV, but no SiII absorption. They also have high column densities when compared to stellar winds.

Previous searches has tried to find the intervening absorbers at $z = 1.38$ and $z = 1.60$. Based on [OIII] emission, Vreeswijk, Møller & Fynbo (2003), found that the absorber at $z = 1.38$ might be located at an impact parameter of 16" from the GRB sightline, which is also consistent with Guillemin & Bergeron (1997) who state that the typical MgII absorber is a luminous galaxy at a fairly large impact parameter. However, there might be a faint galaxy at a small impact parameter as is also seen for DLA systems. In fact the GRB021004 system actually show similarities to a DLA system (Savaglio et al. 2002; Fynbo et al. 2005). Deep HST imaging exists as well, and there are several faint galaxies within 10" of the host galaxy, which might be associated with the absorption systems (Fynbo et al. 2005)

2.2.2 GRB030226

GRB030226 was detected by the *HETE-2* satellite, and the optical counterpart was found approx. 2.5 hours after the burst (Fox et al. 2003 & Shin et al. 2006). It had a magnitude of approx. 18.5 at the coordinates RA.= 11:33:04.92 and Decl. = +25:53:55.6 (J2000) and was a long-duration burst lasting more than 100s (Klose et al. 2004). Observations with Chandra also showed a x-ray afterglow at the same position of the optical transient, thus establishing a connection to the GRB030226 (Pedersen et al. 2004). No host galaxy has ever been found, neither by imaging nor on the basis of emission lines in the spectrum of the GRB (Klose et al. 2004; Jakobsson et al. 2005). The lightcurve of the GRB was achromatic and showed a jet break, i.e. a steepening in the optical light curve, one day after the burst (Pandey et al. 2004). The afterglow showed polarization as well, and all of this indicates that a jet might have been present (Klose et al. 2004; Pandey et al. 2004). From the decay of the afterglow flux, Pandey et al. found that the extinction in the host galaxy is similar to what is seen in starburst galaxies.

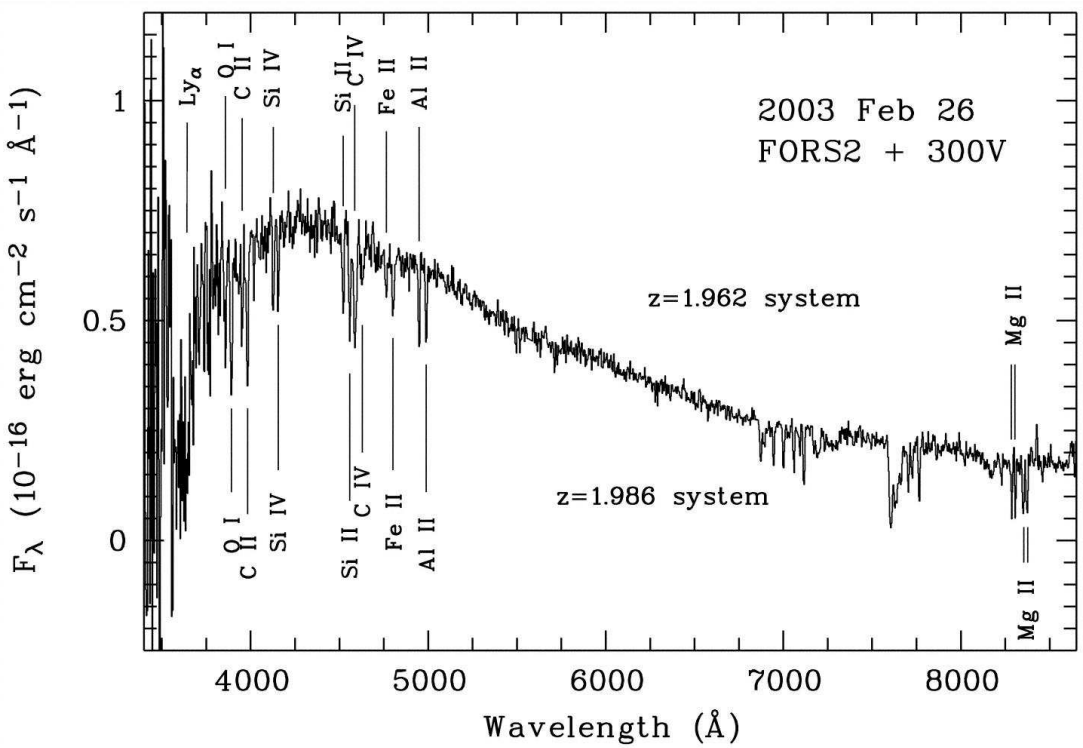

Figure 2.2: Short wavelength part of the afterglow spectrum for GRB030226 taken 5 hours after the burst. The two absorption systems at 1.962 and 1.986 are shown (Klose et al. 2004).

Absorption Systems

Since the afterglow was discovered so rapidly, it was possible to obtain an optical spectrum of it only 5 hours after the burst (see figure 2.2). It displayed a wide range of absorption lines including MgII, FeII, AlII, SiIV and CIV (Klose et al. 2004). On the basis of these lines, they identified three absorption systems at z = 1.042, z = 1.962 and z = 1.986. This makes the redshift of the GRB z = 1.986 or larger (Klose et. al. 2004), where the highest redshift might be due to the absorbing host galaxy. Shin et al. (2006) find an additional absorber at a redshift of z = 1.953, determined from CIV lines. The absorption systems at a redshift of z = 1.962 and z = 1.986 have a velocity separation of 2400 km s^{-1}, and because both systems show traces of highly ionized species of SiIV and CIV, these could possibly be caused by a fast circumstellar wind from the progenitor Wolf-Rayet star moving in a strong magnetic field, very similar to GRB021004 (Klose et al. 2004). The two systems might also be multiple DLAs (Shin et al. 2006). These systems are then very similar to the DLAs towards the line of sight of QSOs given in Ellison & Lopez (2001), where both the velocity separation and the redshift are similar. This might indicate that the two systems are a part of a large scale galaxy structure, as the two absorbers are on the same line of sight within a small velocity separation (Ellison & Lopez, 2001).

The afterglow spectrum also contains a strong Lyα absorber, and this implies that the interstellar medium is dense, possibly close to the redshift of the burst. The redshift has, however, not been determined, only the constraint $1.93 < z < 1.99$.

2.2.3 GRB020813

The *HETE-2* satellite also discovered GRB020813, which was a long-duration burst with a series of pulses. A bright optical transient was discovered 1.9 hours after the burst at RA. 19:46:41.88

Table 2.2: MgII absorption features in GRB030226 (Klose et al. 2004)

Ion	λ_{obs} (Å)	W_r (Å)	z_{abs}
MgIIλ2796.35	5711	0.9 ± 0.1	1.042
	8284	5.0 ± 0.2	1.963
	8349	6.8 ± 0.6	1.986
MgIIλ2803.53	5726	0.5 ± 0.1	1.042
	8305	3.5 ± 0.3	1.962
	8370	5.9 ± 0.4	1.985

and Decl. -19:36:05 (J2000) (Fox, Blake & Price 2002). The optical afterglow was one of the smoothest seen for GRBs (Laursen & Stanek 2003). It had a fading X-ray afterglow as well, and this was observed with the *Chandra* High Energy Transmission Grating System approx. 21 hours after the burst (Fiore et al. 2005).

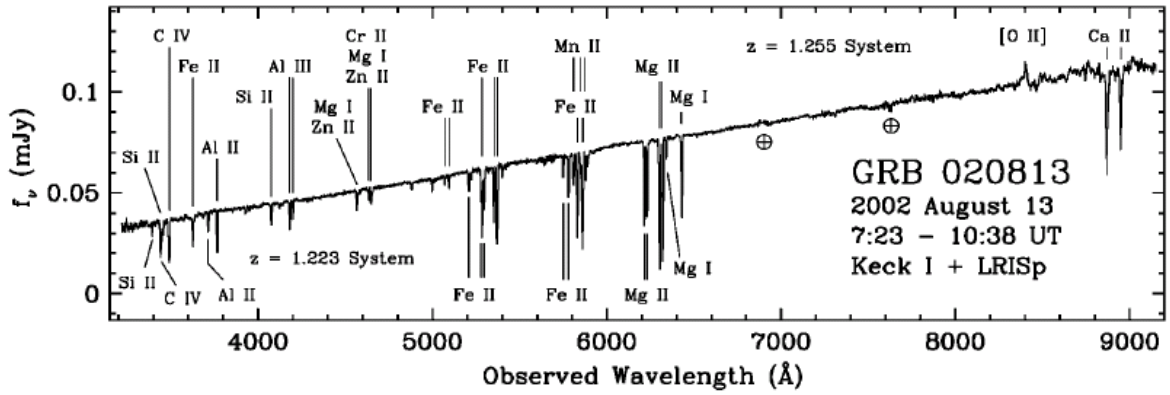

Figure 2.3: Combined spectrum of the GRB020813. The lines for the two absorption systems are marked on the figure. The two encircled crosses are are residuals from the removal of telluric lines (Barth et al. 2003).

Absorption Systems

GRB020813 shows numerous metal absorption lines, and two distinct strong absorption systems at $z = 1.223$ and $z = 1.255$ were detected (see figure 2.3). However, the redshift of the GRB is not high enough for detection of strong high-ionization lines in the afterglow spectrum. An [OII]λ3727 emission line was also seen at $z = 1.255$, which is most likely due to the host galaxy. The system at 1.255 actually consists of three absorption systems separated by 0 km s^{-1}, -106 km s^{-1} and -306 km s^{-1} compared to the host galaxy i.e. they are blueshifted (Fiore et al. 2005). The two systems closest to the host galaxy have strongly blended lines, except for an FeIIλ2374 line. These systems are probably formed in the local environment of the GRB. The lowest redshift system has a velocity distance of approx. -4200 km s^{-1} from the host galaxy. Fiore et al. 2005 remark that the probability of finding a MgII absorber within this velocity range is less than 1%, and that it is similar to GRB021004 where the shift is approx. 3000 km s^{-1}, thus suggesting that the local environments might be similar. There is of course still a possibility of the system being an intervening absorber.

Table 2.3: MgII absorption features in GRB020813 (Fiore et al. 2005).

Ion	λ_{obs} (Å)	W_r (Å)	z_{abs}
MgIIλ2796.35	6216.93	1.34 ± 0.03	1.2234
	6300.13	0.55 ± 0.03	1.2529
	6304.72	2.38 ± 0.03	1.2550
MgIIλ2803.53	6232.85	1.36 ± 0.03	1.2234
	6316.13	0.30 ± 0.03	1.2529
	6321.11	2.19 ± 0.03	1.2550

On the basis of *Chandra* X-ray data, Butler et al. 2003 detect metal emission lines from e.g. S XVI, that are usually produced in the nucleosynthesis of massive stars before a supernova event. These lines show variability in time and also a large blueshift, and are thought to arise from a supernova that occurred 0.1-10 yr before the GRB. The afterglow also came later than the burst itself, suggesting the beaming effect of a jet. However the validity of these lines are still strongly debated.

Chapter 3

Observations

3.1 Telescope and Detector

The scientific observations for my thesis were carried out with the Very Large Telescope (VLT) operated by the European Southern Observatory (ESO). It is located at Paranal in Chile and consists of an array of four telescopes, each with a mirror size of 8.2 m. It is possible to use all of the four telescopes for the same observation, which can be compared to using one telescope with a mirror size of 16 m. All af the telescopes have an alt-azimuth mount making a full sky coverage possible. The VLT uses active optics to minimize optical aberrations such as coma and astigmatism. Different instruments can be mounted in various focii (Cassegrain, Nasmyth or Coudé) on each of the four telescopes, depending on the type of observation. For my thesis the observational setup was with the instrument FORS2 mounted on the ANTU telescope in Cassegrain focus. FORS is a visual and near UV FOcal Reducer and low dispersion Spectrograph and operates in the wavelength range from 330 nm to 1100 nm.

Figure 3.1: ESO VLT at Paranal

Several observing modes are possible e.g. direct imaging and multi-object spectroscopy with movable slits (MOS). However, longslit spectroscopy (LSS) has been used here. In this mode a mask containing nine slits, each with a slit length of $6.'8$, is placed in the focal area of FORS2. The slits have different widths in the range of $0.''28 - 2.''5$.

Two types of collimators can be used, giving either standard or high resolution. For my data, the standard collimator was used yielding a pixel scale of $0.''25$/pix. In the parallel beam, different filters and grisms can be put into the light beam. As my data are spectroscopic, the choice of grism is important and depends on the target field; in particular the redshift of the MgII absorbers. I will elaborate on the specific choice in the following sections.

FORS2 has a mosaic of two MIT CCDs, each with a size of 2k×4k (for a small review on CCDs, read-out-noise and gain see Appendix A). Each pixel is 15×15 μm giving a pixel scale of $0.''25$/pixel (or $0.''125$/pixel for the high resolution collimator). The lower CCD is rotated by 0.8 degrees and shifted 30 μm compared to the upper 'master' CCD, yielding a gap of 480 μm. The field of view is $6.'8 \times 6.'8$ by use of the standard collimator. With FORS2 the center of the field of view will fall on approx. $Y \sim 260$ on the upper master CCD i.e. CCD1. Therefore CCD1

is the most interesting, since I am searching for galaxies at small impact parameters. CCD1 has a read-out-noise of 2.9 e^- and a gain of 0.7 e^-/ADU. For details of the properties of FORS2, see table 3.1.

Table 3.1: Properties of FORS2

	Standard Resolution	High resolution
Collimator Focal Length	1233 mm	616 mm
Camera Focal Length	280 mm	280 mm
Final F-ratio	3.13	6.25
Field of View	$6.'8 \times 6.'8$	$4.'25 \times 4.'25$
Pixel Scale	0."25/pixel	0."125/pixel
Read Out Noise	2.90 e^-	2.90 e^-
Gain	0.7 e^-/ADU	0.7 e^-/ADU

3.2 Observational setup

The observations were a part of the two ESO programmes P75A-0826 and P77A-0312 with P. Vreeswijk as PI and the collaborators P. Møller, J. P. U. Fynbo and S. Ellison.

Before the scientific observations, preimaging took place, where 8 imaging frames - each with an exposure time of 150 s in the R band - were obtained for each target field. These frames were used to search the target fields for any potential absorbers, i.e. faint galaxies at small impact parameters relative to the GRB site. From these the slit alignments could be determined, to cover interesting objects in each field. All of the spectroscopic observations were made with a 1" wide slit. The slits were also chosen to cover where the GRB afterglow was. This is to search for absorption systems lying close to the sightline of the GRB, or the host galaxy if the wavelength range of the science frames permits it. Since the absorbing galaxies are very faint a blind offset from a reference star was used to get the target galaxies on the slit. For determination of the reference star, as well as well as calculating the distance parameters to the actual slit positions, the preimaging frames were used as well.

The ESO programmes were a part of the service observation program and thus all of the observations were carried out by the staff at ESO Paranal, where the details of the observations were provided to them. These details include all of the observational setup, e.g. target, exposure time, grism, slit position angle, and which kind of calibration frames, as well as finding charts and reference star offsets. The preimaging were a part of this programme as well and were carried out before the actual spectroscopic observations. All observations were made prior to my entry in the project.

For the various target fields different setups have been used, depending on the redshift of the absorber, and the following subsections give an overview of the observational setup of the target fields, as well as the slit alignments. Details for all of the observations are given in tables 3.2, 3.4, and 3.5.

GRB021004

The field of GRB021004 contains several interesting objects at a small impact parameter. Figure 3.2 shows how the slits were placed to cover these. The alignment of the slits are given in position

angles, i.e. amount of degrees East of North. The position angle 70.37 also covers a galaxy at the impact parameter 16", as this is the galaxy that were found in previous studies to have the same redshift of the absorber at $z = 1.38$ (Vreeswijk, Møller & Fynbo 2003). This object was chosen in order to confirm the redshift by spectroscopy. However there has never been searched for the $z = 1.3806$ absorber at smaller impact parameters, and thus this, as well as the $z = 1.6039$ absorber, might be among the faint galaxies within approx. 5" of the GRB covered by one of the slits.

In order to meet these scientific requirements, the grism was chosen to cover the [OII]λ3727.26 emission at the lowest redshift of the absorbers in the target field. This corresponds to the absorber at z=1.3806, and at this redshift the [OII] line is redshifted to 8873 Å. The grism 600z was chosen as it has a central wavelength of 9010 Å and covers the wavelength range 7370 - 10700 Å. The slits were placed at the position angles 70.37, 30.50 and 91.41 as seen in figure 3.2. No observations were made for the slit position angle 152.51, probably due to bad weather. The observational setup is shown in table 3.2. Note that there is only one science frame for the position angle 70.37.

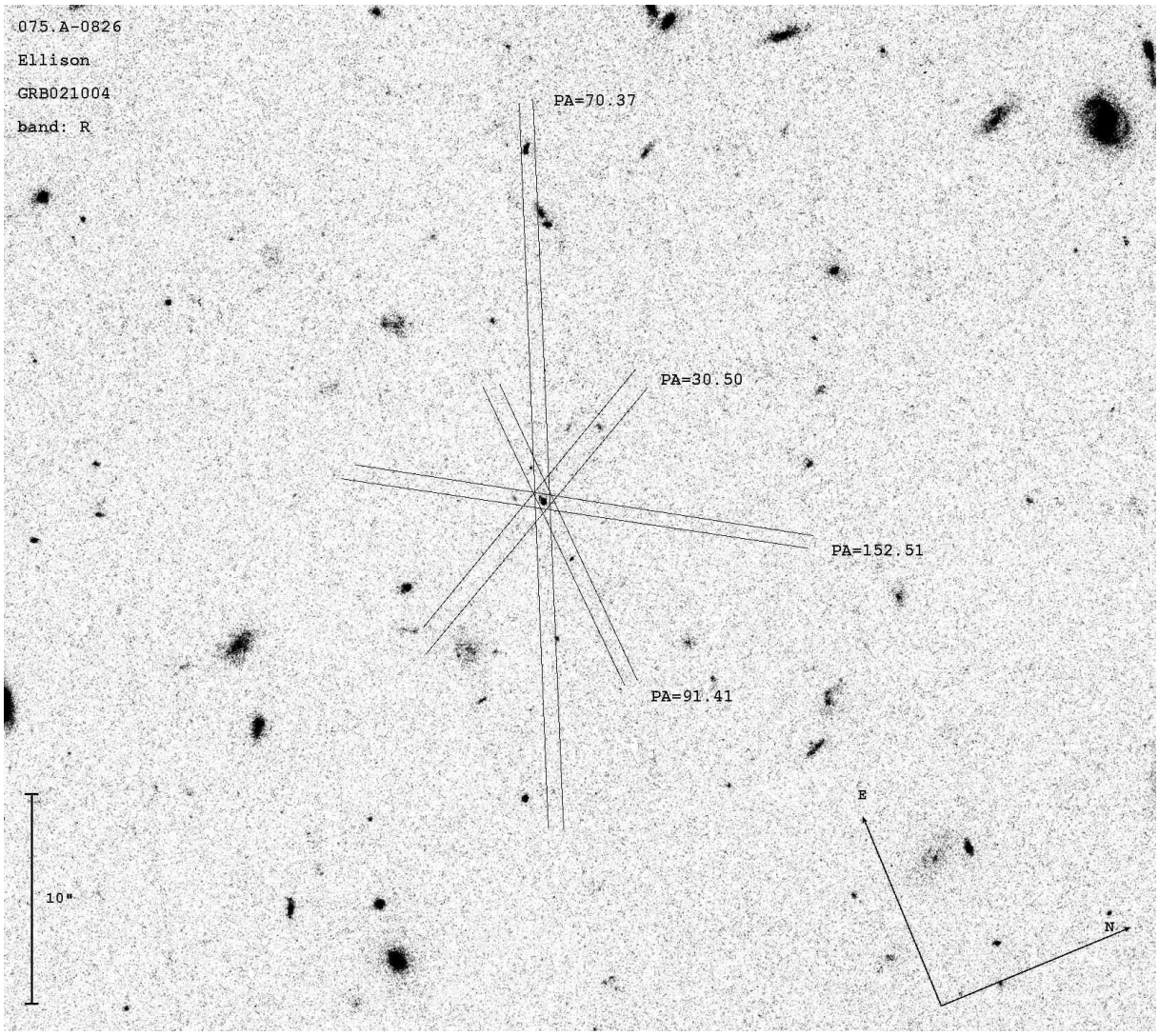

Figure 3.2: Slit alignment for GRB021004

Table 3.2: Scientific observations of GRB021004

Date	Position Angle Degrees E of N	Grism	Filter	Slit (″)	Exposure Time (s)
2005-07-02	70.370	600z	OG590	1	1 x 2099
2005-07-05	30.500	600z	OG590	1	2 x 1474
2005-07-06	30.500	600z	OG590	1	2 x 1474
2005-07-09	91.410	600z	OG590	1	1 x 1474
2005-07-09	91.410	600z	OG590	1	1 x 878.
2005-07-10	91.410	600z	OG590	1	4 x 1474

Table 3.3: The Characteristics of the grisms for the 1" wide slit

Grism	Filter	λ_{range} (Å)	Resolution	Dispersion (Å/pixel)
600z	OG590	7370-10700	1390	0.81
1028z	OG590	7730-9480	2560	0.42
600RI	GG435	5120-8450	1000	0.83

GRB030226

There is only one intervening absorber for this field at $z = 1.042$, and there are several possible candidates for the galaxy counterpart. Of special interest are the two galaxies on the slit with position angle 119.08 in figure 3.3. They are on either side of the GRB within a radial distance of 5". Figure 3.3 also shows the reference star for the slit offsets as well.

The grism was chosen to cover the [OII] emission for the absorbing system at z=1.042 and the chosen grism, 600RI, is suitable with a wavelength range of 5120-8450 Å. The central wavelength of the grism is 6780 Å. However due to manufacturing errors this grism shifts the spectrum on the detector in the *Y*-direction by approx. 272 pixels since it tilts the light beam. With the use of the standard collimator this causes the upper 21" to fall beside the CCD and is thus not observable (FORS1+2 User Manual, 2006). This should not cause much problems though, since the target should be placed at $Y \sim 260$ and I am searching for objects close to this value. All the science frames have an exposure time of 1474 s, which means that the total integration time for the combined images at the same position angle is approx. 1.5 hours. The slits have been aligned at 119.08, 35.79 and 155.72. The encircled star in figure 3.3 is the offset star. For wavelength calibration He/Ne/Ar, as well as HgCd lamps were used.

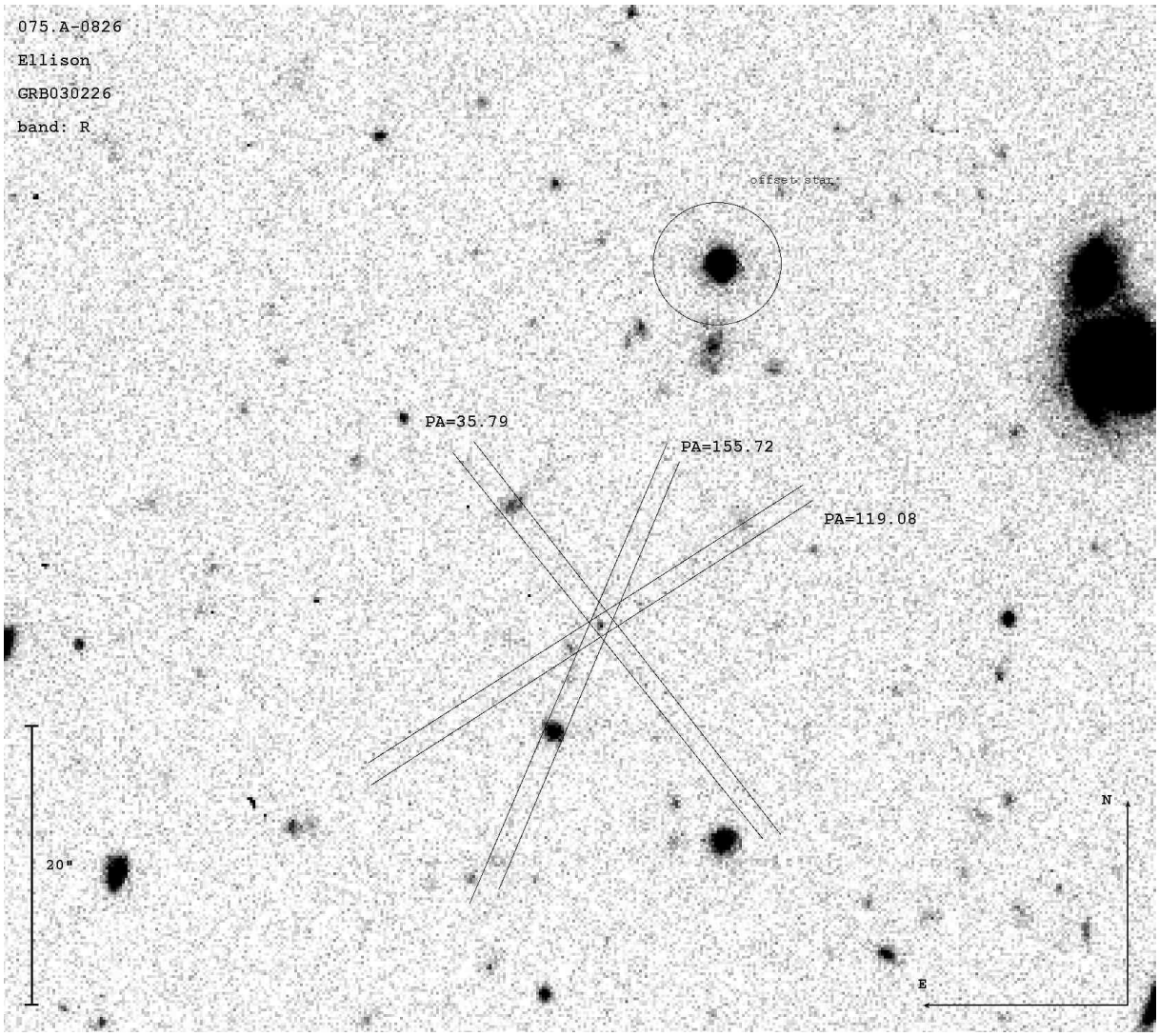

Figure 3.3: Slit alignment for GRB030226

Table 3.4: Scientific observations of GRB030226

Date	Position Angle Degrees E of N	Grism	Filter	Slit (″)	Exposure Time (s)
2005-04-02	119.080	600RI	GG435	1	2 x 1474
2005-04-03	119.080	600RI	GG435	1	2 x 1474
2005-04-03	35.790	600RI	GG435	1	2 x 1474
2005-04-04	35.790	600RI	GG435	1	2 x 1474
2005-04-06	155.720	600RI	GG435	1	4 x 1474

GRB020813

This GRB has one absorption system at $z = 1.223$. The host galaxy is clearly visible in figure 3.4 and should show up in the spectra as well. As the absorption system and the host galaxy are fairly close (the host galaxy is at $z = 1.255$) they might be covered by the same grism and the redshift of the host galaxy might be determined as well. The galaxies in the vicinity of GRB020813 are shown in figure 3.4 as well as the slit alignments. The object of special interest are the ones within 5" of the GRB site.

The [OII] emission of the absorption system is covered by grism 1028z with a wavelength range of 7730-9480 Å.

Table 3.5: Scientific observations of GRB020813

Date	Position Angle Degrees E of N	Grism	Filter	Slit (″)	Exposure Time (s)
2006-07-17	5.000	1028z	OG590	1	2 x 1316
2006-07-19	-39.000	1028z	OG590	1	4 x 1316
2006-07-19	27.000	1028z	OG590	1	2 x 1316
2006-07-21	27.000	1028z	OG590	1	2 x 1316

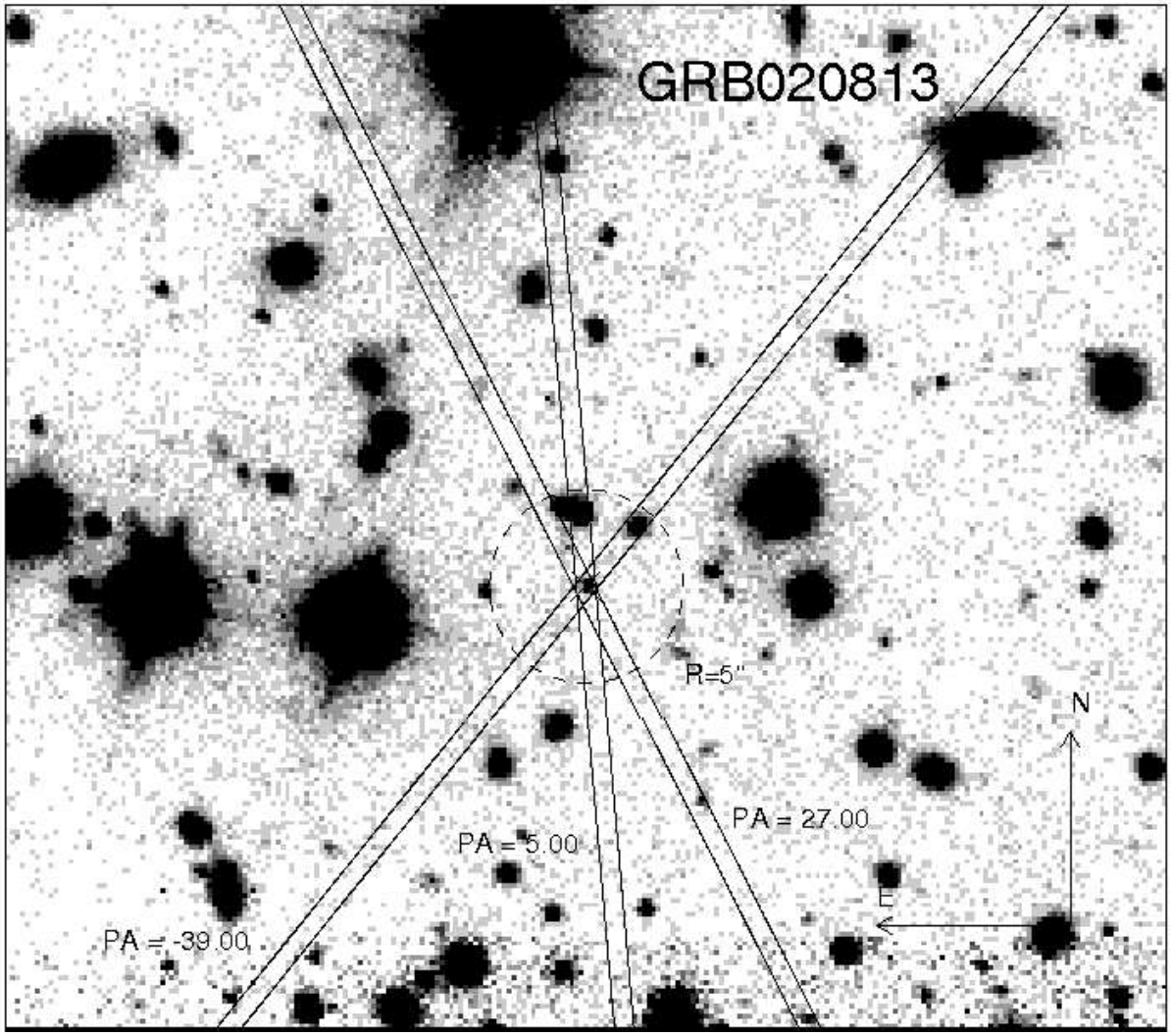

Figure 3.4: Slit alignment for GRB020813

Chapter 4

Calibration Methods

One of the major parts of my thesis was to reduce, calibrate the raw data, and analyze the reduced data from FORS2. In this chapter I will outline how I performed the various steps and which tools I used.

4.1 Image Reduction

The raw data consists of science frames and calibration frames i.e. bias, flatfields as well as arcs. Firstly, all of the data is sorted into the various observing nights. This is done because the science frames need to be reduced by use of the calibration frames taken at the same night (for bias this is not as important). Not all nights are the same, as for instance the weather might be different, and as is also seen for normal imaging, atmospheric disturbances causes variations in the seeing. If the calibration frames for the corresponding night is used, this will yield the most precise reduction. On some of the nights it has either only been possible to obtain science frames or calibration frames and thus I have chosen to use the calibration files from the day closest to the science observation, providing the data were good.

4.1.1 Cosmic Ray Removal

One important aspect of data reduction is the removal of cosmic rays. They are always on science frames and to a less extent on calibration frames such as flatfields and can affect several of the pixels in an image. The longer exposure, usually the more cosmics as the probability of one hitting the detector is higher. The most common way of removing them is by obtaining several science frames and combining these by use of a median or σ-clipping. This will usually remove most of the cosmics. However in this case, I am interested in a deep as possible image, and will thus add the science frames together. Cosmics will therefore stay on my science frames, if not removed before they are combined. For this process I used the program *L.A.Cosmic* by Pieter van Dokkum (van Dokkum 2001) made for spectroscopy. This program uses an algorithm based on a Laplacian convolution, designed to reject cosmic rays by detection of the sharpness of the edges of the cosmic ray. If the contrast between the entire cosmic and its surroundings would have been used instead, poorly sampled objects could have been removed as well. When a cosmic is removed the program uses the median of the surrounding pixels as a replacement (van Dokkum 2001). As setup it is important to use the properties of the detector as well as a significant amount of iterations in order to get the optimal cosmic removal, so I set the program to run with the parameters for the FORS2 CCD i.e. a read-out-noise of 2.9 e^- and a gain of 0.7 e^-/ADU and I used four iterations for each science frame.

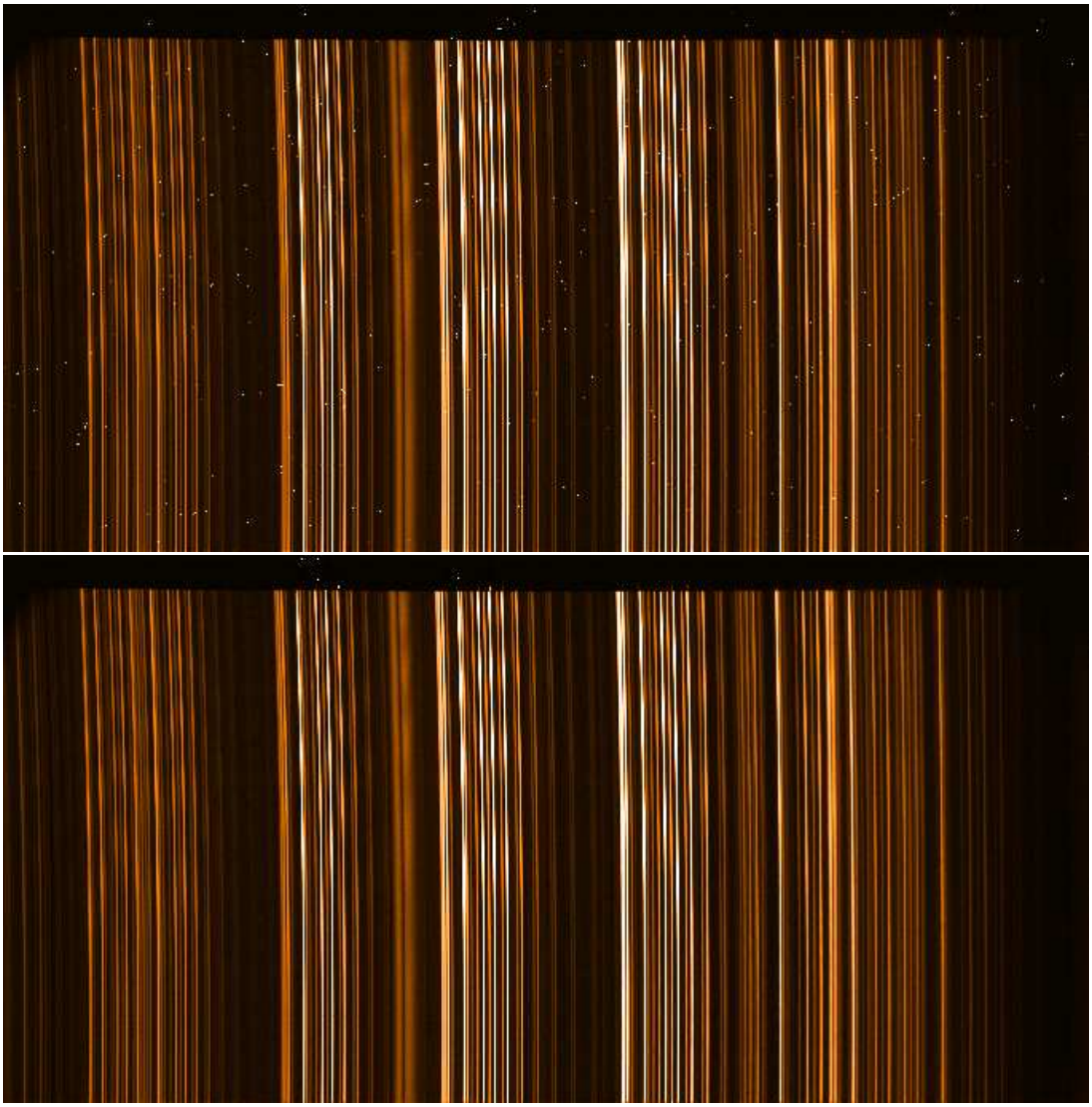

Figure 4.1: One of the science frames for GRB020813 before (upper) and after (lower) the cosmic ray removal.

4.1.2 Bias and Flatfielding

For optimal correction for bias I subtracted the bias level, given in the overscan region from each bias frame. After this, all of the bias frames were combined by use of the median in *IDL*. For each science and calibration frame both the overscan and the combined bias frame are used. This makes sure that there is a correction for the bias pattern across the CCD, and not just the overall bias level. For this step I used *IRAF* and the task **ccdproc**. The valid overscan region for the bias frames is manually put into the parameter list, and the task averages the overscan along the readout direction, hereby making an overscan vector. I used an interactive curve fitting when running the script, and thus fit a smoothing function to the overscan vector. Here it is possible to discard data-points with a large dispersion such as sky lines. I fitted a Chebyshev polynomial of the order 10 to the overscan vector to obtain a good rms (root mean square). This process, as well as subtraction of the combined biasframe, were done for all the calibration frames as well as the science frames.

Flatfield correction is done in a different way for spectroscopic data than for imaging. When obtaining the flats the grism and filter is still in, and thus the flatfield frames contain a spectrum

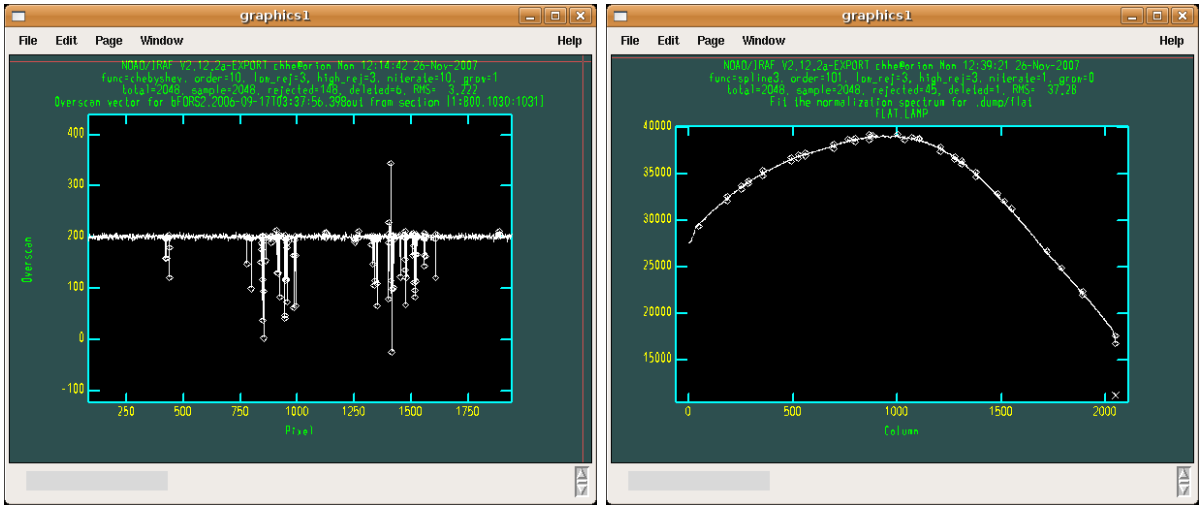

Figure 4.2: Bias and flatfielding for GRB020813 in IRAF. Left: Fitting the overscan vector to a science frame for GRB020813. It is possible to delete any points and as such I removed points with a large deviation from the fit. Right: Fitting the response curve for the flatfields.

of the lamp (or sky if skyflats are used) as well as transmission variations with wavelength for the given setup. In order to remove these effects properly an average of the lines (or columns) across the dispersion and within the aperture is normally used. This provides an estimate of the spectrum. To remove noise a smooth curve is fitted to the flat spectrum - called the response curve. This function is then divided back into all of the lines within the aperture. It is also important that the section used for determination of the response curve covers the scientific targets on the slit. Otherwise the flatfielding will not be optimal. The task for longslit flatfielding is **response** in the **longslit** package. I fitted the response curve - a Chebyshev polynomial of the order 101 - interactively and set the task to reject anything above and below 3σ of the curve. To get a good fit I also used about 10 iterations. The formed response flatfield images are then combined by use of the median, and each science frame as well as the wavelength calibration frames are then devided by the combined flatfield frame. The science frames are thus reduced, but in order to get a reference to wavelength i.e. convert the pixelscale to wavelength, a wavelength calibration is needed.

4.1.3 Wavelength Calibration

I also performed the wavelength calibration in *IRAF*, and used the tasks **identify**, **reidentify**, **fitcoords** and **transform**. The first task is used to identify the lines of the respective arc lamp used for the observations. A full list of the lines for the various grisms for FORS2 was found in the ESO FORS2 manual. This task is interactive as well and here it is possible to mark the emission lines and state their redshifts. This is then compared to the list of emission lines. A fourth order Chebyshev function is then fitted to the input wavelength coordinates. This polynomial is a function of pixel coordinate and thus there is a link between the pixel coordinate and wavelength. It provides a list of where the features are in the arc spectrum. The second task **reidentify** can identify the same features i.e. emission lines from the **identify** but additional features can also be determined from the line list. Again a polynomial fit is used and the resulting data is written to a textfile. **fitcoords** fits a function of the image coordinates to the wavelength coordinates (and the Y coordinate is unchanged) thus creating a 'coordinate map'. All the information regarding the fit is saved in a text file to be used for the final step.

The last process of the wavelength calibration is to convert all of the science frames to the

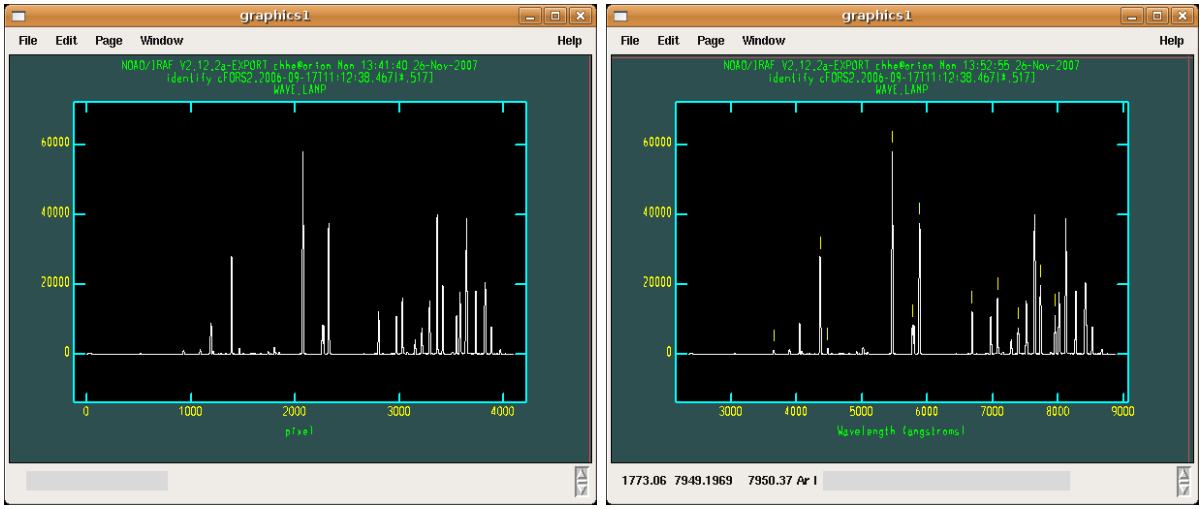

Figure 4.3: Determination of emission lines for wavelength calibration. The left image is before any emission lines have been put in and thus the scale is still pixels. In the right image some of the emission lines have been determined and the image scale has been converted to wavelength.

right wavelength. Where the previous tasks dealt with the arc frames alone, the **transform** task uses the coordinate maps made from the previous task and converts the original X- Y-coordinate set to Wavelength- Y- coordinates. The typical rms for the wavelength calibration is approx. 0.25 pixels. This is done with all of the science frames and afterwards they are ready to be used for analysis.

4.2 Analysis

In this section I will explain how the reduced science frames were used to determine the redshifts of the galaxies positioned on the slit. Several steps needed to be performed before the actual wavelength determination could take place. Firstly the science frames needed to be combined and I used background subtraction as well to make the emission lines clearer. For most of the analysis part I used *ESO-MIDAS*, as this has some nice features and tools.

4.2.1 Combining the Science Frames

Since I am searching for galaxies that are very faint, I want to obtain an as deep as possible combined spectrum. In order to achieve this I have for every target, combined all of the science frames for each separate position angle. The trace of the objects on the slit will, however, not be in the same position for every science frame so I need to make an offset before combining the images. For finding a reference for this offset I used *ESO-MIDAS*. By averaging the columns in a given wavelength range avoiding skylines, it is seen where the traces from various objects are placed on the CCD i.e. their Y-coordinate (see figure 4.4). I then used a strong trace of e.g. a luminous galaxy as the "reference point" on each of the science frames. The precise Y-coordinate is found by use of the tool **cent/gauss**. This fits a gaussian to the trace and finds the corresponding center of the curve. Provided with the shift in Y, I cut out each science frame in a specified range, to make them all have the traces at the same place, as well as making sure all of the frames have the same dimensions. To keep a small overscan region in the bottom of the images from entering the combined frame, I made the selected range begin above this region i.e. at a higher Y. For the science frame with the reference trace positioned at the lowest Y, I

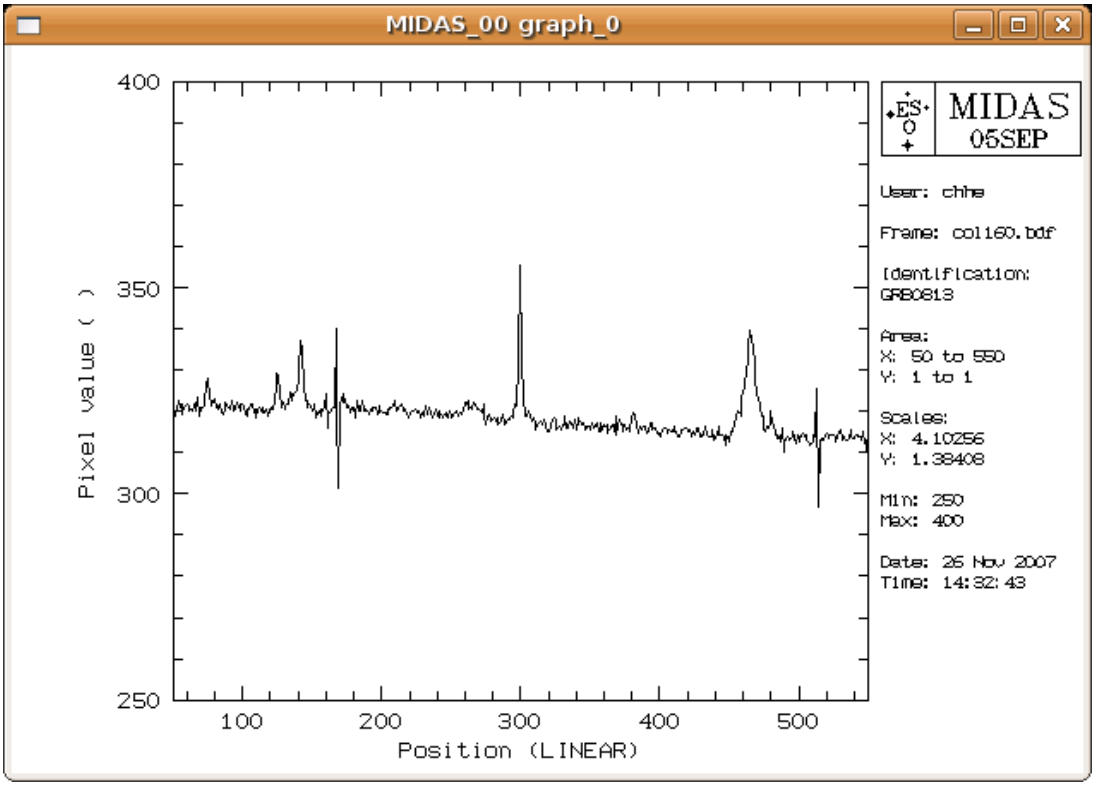

Figure 4.4: The average of the columns between 500 and 800 pixels for the position angle 27.00 for GRB020813. It is seen that there are several traces which can be used as a reference. However I chose the strongest trace at the position 465 in this frame.

used the range [*,10:900] (with [xrange,yrange] and * meaning the whole range), and the range of all the other frames were calculated from this, i.e. [*,10+shift:900+shift]. For cutting out the selected region I used the *IRAF* task **imcopy**. After this step I added all of the science frames together by use of the task **imcalc**. This final step provides the reduced and combined science frames (see figure 4.5).

For some of the GRB sightlines it has also been interesting to see whether the host galaxy or a very faint galaxy lying almost at the sightline might be found. For e.g. GRB030226 the host galaxy has not been found and thus for this field it is of special interest to go deep where the GRB went off. In this case I have added the already combined science frames for each position angle, with a reference point in the Y-coordinate where the GRB happened. This reference point is, however, not easy to find as there is of course no trace at that position. Instead I have used deep images of the GRB field taken when the afterglow of the GRB was still visible. Then I have calculated the scaling factor between the deep image and the acquisition image I had of the field, thus providing a sort of measure of distance between the objects on the slits. This made me able to determine at approx. which Y-coordinate the GRB should have happened for each position angle. Adding the frames together afterwards was done the same way as before. The combined image have a lot of traces as this image is a combination of several slit position angles. However the reference point is of course still the same and this provides the position of where the possible trace of the GRB host or intervening absorber should be.

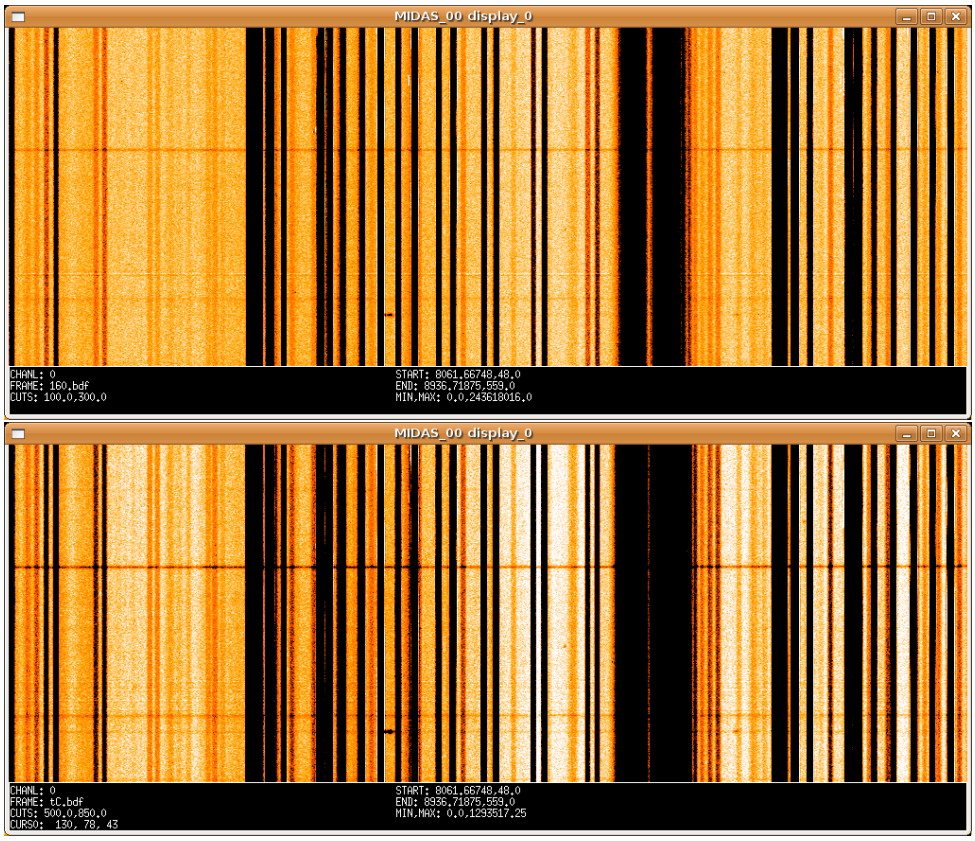

Figure 4.5: Upper: One of the science frames for GRB020813 at position angle 27.00 Lower: All of the science frames for this position angle have been combined. Notice that the traces have become stronger.

4.2.2 Background Subtraction and Smoothing

My goal is to determine the redshift of as many of the objects close to the respective GRB sightline as possible. As most of the galaxies are faint it can be hard to find any emission lines as they will kind of 'blend' in with the background. Thus I have subtracted the background around the trace of each of the galaxies to make the emission lines stand out more clearly in the 1D spectrum. It was also a clear choice not to extract the spectra by use of e.g. *IRAF*. The objects are so faint that it is hard to tell an emission line from the noise, but by use of the 1D spectrum these lines are more easily detected. For background subtraction I used the task **background** in *IRAF*. This task fits a function to the column background and subtracts this from the image. For the fitting I used a fifth order spline3 function and the rejection limit is set to 4.5σ.

One more way to make the emission lines clearer is to use a smoothing filter on the image. This way the pixels are replaced by an average of the surrounding pixels by use of a linear filter and this causes the noise to be reduced. Mathematically this means that a convolution by the filter function $F(i,j)$ on the image $I(m,n)$ is performed, thus yielding the smooth image (ESO-MIDAS User Guide 1998):

$$S(m,n) = \sum_{i=-k}^{k} \sum_{j=-l}^{l} I(m-i, n-j)F(i,j).$$

For comparison between the un-smoothed and smoothed image see figure 4.6. The smoothed image is not used for the error estimations though, because this would make the noise appear

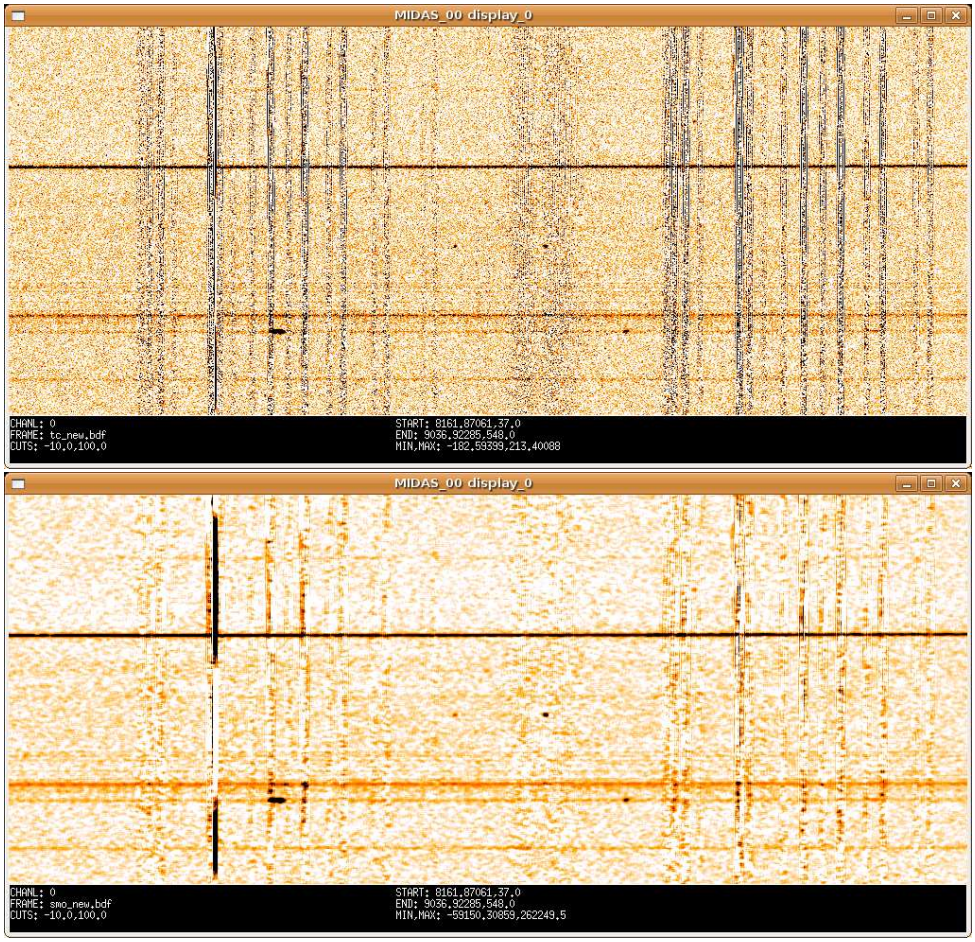

Figure 4.6: Upper: The combined frame for GRB020813 at the position angle 27.00, where I have subtracted the background. Compared to the lower image in figure 4.5, the lines are already more clear. Lower: The same frame as the upper, but here the image has been smoothed. The emission lines stand out clear for the second lowest trace (which is in fact the host galaxy of GRB020813).

smaller than it actually is (see section 4.2.4).

4.2.3 Determining the Redshifts

The emission line I am searching for is the [OII] line. However, several other metal lines might be seen as well. These lines are listed in table 4.1.

If there are several emission lines present, it is a matter of finding the metal lines that will yield the same consistent redshift. The redshift can be determined by the usual equation:

$$z = \frac{\lambda_{obs} - \lambda_{rest}}{\lambda_{rest}}$$

To determine the wavelength of a line I used the *ESO-MIDAS* task **cent/gauss**. This task fits a gaussian to the line and determines the center of the line as well as the uncertainty.

For the part of the spectrum containing sky lines, it is not easy to determine precise wavelengths unless the lines are strong. The sky lines give a large uncertainty as they cannot be removed. By subtraction of the background they have been minimized, but the noise in that part of the spectrum is still large.

Table 4.1: Possible Metal Emission Lines (Prochaska et al. 2004).

Ion	λ_{rest} (Å)
[OII]	3727.26
[NeIII]	3869.84
[NeIII]	3970.00
Hδ	4102.90
Hγ	4341.69
[OIII]	4364.44
Hβ	4862.70
[OIII]	4960.29
[OIII]	5008.24
Hα	6564.63

If there is only one emission line in the spectrum, it is not possible to securely identify the metal line, and hereby the redshift, as the line might often be any of the proposed lines. The reason for only one line being present, could be that the object is so faint, that only the most prominent line in the given wavelength range of the science frame is visible. Sometimes a trace is not seen at all. It might also be a distant Lyα emitter which just happens to lie close to the line of sight to the GRB.

Another scenario is that the lines are so faint, that they are hard to distinguish from the noise. As most of the objects are faint this was often the case, so here I tried to find out whether there were any possible lines, especially where any [OII] emission of the absorbers should be. The uncertainty of the line is then large as the S/N is very small.

4.2.4 Error Estimation

To give a valid approximation of how strong a given emission line is, the signal-to-noise ratio (S/N) is normally used. This describes how high the signal of the line is compared to the noise. The signal is simply the flux in a given aperture covering the emission line. For this determination I used the **mag/circ** task in *ESO-MIDAS*. Here it is possible to state the precise aperture size in pixels. The noise is given by the standard deviation for the given aperture size used for determination of the flux:

$$N = std.dev(aperture) = \sqrt{N_{pixel}} \times std.dev(pixel)$$

The standard deviation per pixel is determined by use of the *ESO-MIDAS* task **stat/image** which calculates various statistics in a given range of the image. I chose this square region to be very close to the emission line e.g. right above, as the statistics are not he same all over the image. The S/N in units of σ is then given by:

$$S/N = \frac{Flux(aperture)}{std.dev(aperture)} = \frac{Flux(aperture)}{\sqrt{N_{pixel}} \times std.dev(pixel)}.$$

For a line to be significant, it should have a $S/N > 5\sigma$.

The uncertainty in the wavelength, and hereby the redshift, consists of both a systematic uncertainty from the wavelength calibration and a random uncertainty from the determination

of the wavelength by a gaussian fit. The systematic uncertainty can be estimated by the rms of the wavelength fit combined with the dispersion for a given grism:

$$\delta\lambda_{wave.calib.} = rms(wave.fit) \times disp(grism)$$

When using the Gaussian fit of the emission lines in *ESO-MIDAS*, the task provides the uncertainty as well. The total uncertainty in λ is a combination of the two:

$$\delta\lambda_{total} = \sqrt{(\delta\lambda_{wave.calib.})^2 + (\delta\lambda_{gauss.fit.})^2}$$

This uncertainty in the observed wavelength, contribute to an uncertainty in the redshift. As there is only an uncertainty in the observed wavelength, the uncertainty in redshift is thus given by:

$$\begin{aligned} \delta z &= \sqrt{\left(\frac{\partial z}{\partial \lambda_{obs}} \cdot \delta\lambda_{obs}\right)^2} \\ &= \frac{1}{\lambda_{rest}} \cdot \delta\lambda_{total} \end{aligned}$$

The uncertainty in the wavelength was usually not higher than 1 Å, thus the uncertainty in the redshift was around 10^{-4}. The largest uncertainty was therefore not in the calculation of the redshift, but in the validity of the lines instead. This is especially evident if only one line is present.

4.2.5 Objects on the Slit

Now that the redshifts have been determined for various objects on a slit it is of course evident that one needs to known exactly which objects on the sky they are. For this determination several acquisition images for each position angle have been made during the observing run. These include both sky and slit acquisitions. For the slit acquisition the objects on the slit are not the targets, since these are so faint that they are not possible to see on acquisition images, which usually have a short exposure time. Instead it is the reference star, used for the blind offset, that is on the slit. Where it is not obvious which objects are on the slit (e.g. in the case of luminous galaxies giving a strong trace) I have used *ESO-MIDAS* to blink the sky and slit acquisition images as well as the combined science frame for a given position angle against each other. However, the acquisition image containing the slit needs to be shifted in the *X*-direction compared to the sky acquisition in order to cover the right objects (otherwise it will cover the slit offset reference star). The process of determining the objects on the slits is shown in figure 4.7.

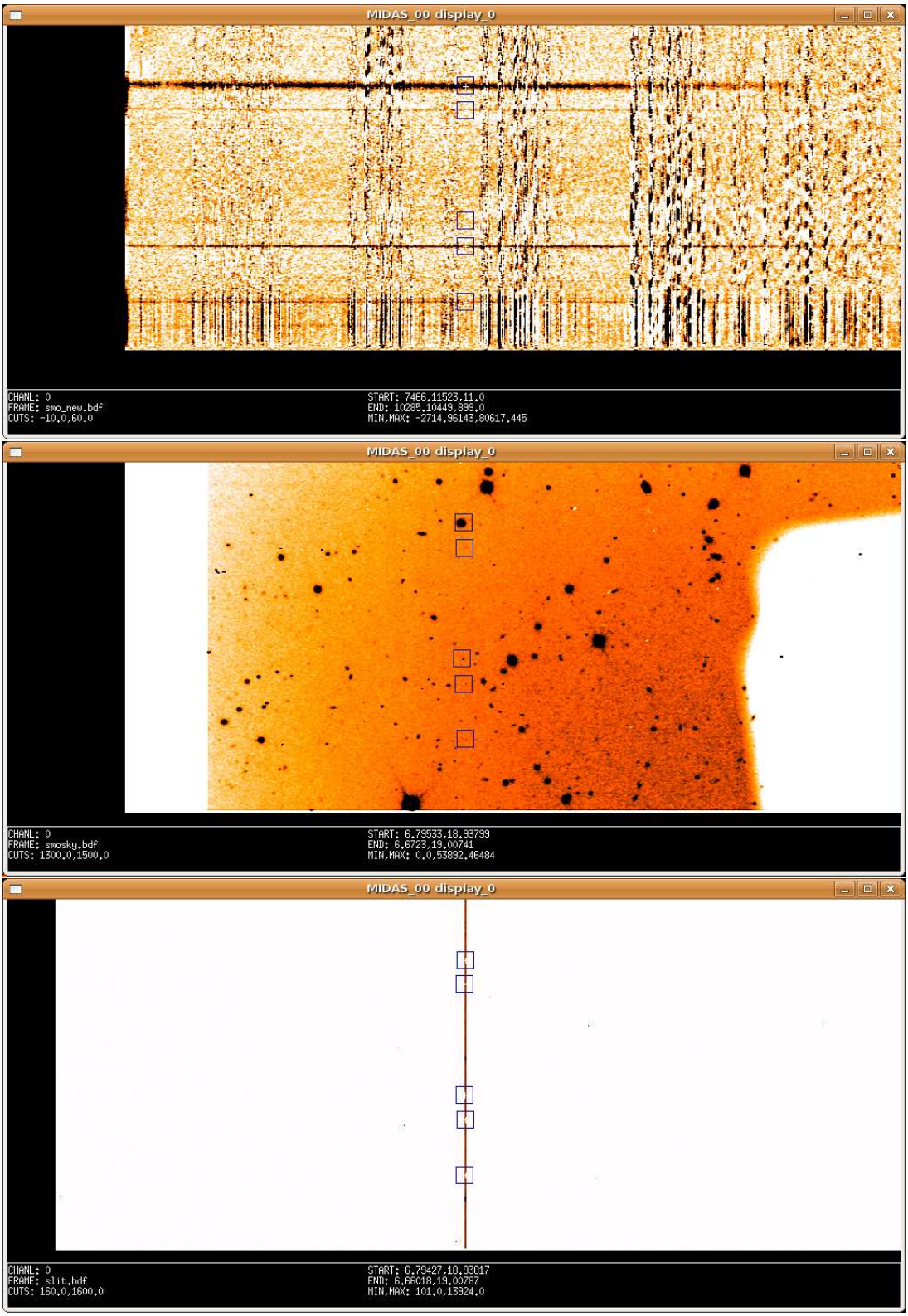

Figure 4.7: Determining which object are on the slit for GRB021004 at the position angle 91.41. The upper panel shows the combined science frame, the middle panel shows the sky acquisition frame and the bottom panel shows the slit. Notice the marks on all three panels are at the same place.

Chapter 5

Redshift Determination

In this chapter I will give all of the determined redshifts and results I have found for the different target fields.

5.1 GRB021004

GRB021004 contains two intervening absorbers at $z = 1.3806$ and $z = 1.6039$ respectively (Møller et al. 2002a). There are several possible candidates for the galaxy counterpart and these are described in section 3.2. The observational setup, providing a wavelength range of the science frames of approx. 7370-10700 Å, is optimal for observing the [OII]λ3727.26 emission line for both the $z = 1.3806$ and $z = 1.6039$ system. However, the absorption systems at $z = 2.2983$, $z = 2.3230$, $z = 2.3292$, as well as the host galaxy at $z = 2.3351$ can neither be detected in [OII] or Lyα, as these lines are outside of the wavelength range.

5.1.1 Emission Line Determination

Position Angle 91.41

For this position angle there is a faint trace of the host galaxy (marked in figure 5.1). Right above there is a faint trace of the galaxy marked with 1 in figure 5.10. The galaxy marked with 2 in this figure show no visible trace. For both galaxies there are no clear emission lines making the redshift determination impossible. As I am searching for [OII] emission from the two absorption systems, I have shown where these lines should be for galaxy 1 and 2 in figure 5.2. There are, however, no lines present.

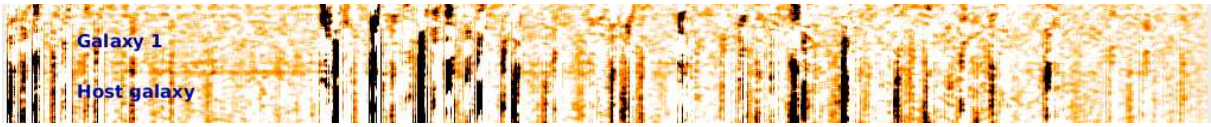

Figure 5.1: Position angle -91.41. The upper trace is galaxy number 1 in figure 5.10. The one below is the GRB021004 host galaxy. The trace of galaxy 2 is not visible. No emission lines are determined.

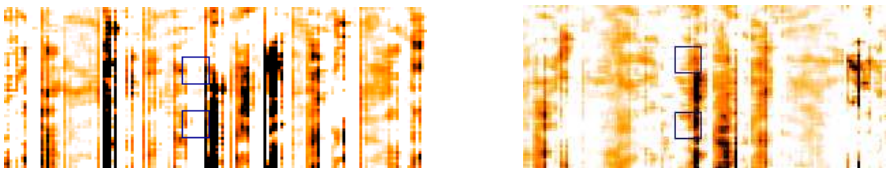

Figure 5.2: Search for [OII] emission of the two absorption systems. Left Panel: The blue squares show where the [OII] emission lines should be for the absorber at $z = 1.3806$. Right Panel: Again I have marked where the [OII] emission should be; this time for the absorber $z = 1.6039$.

Position Angle 30.50

This position angle shows the same tendency as the previous. There are no strong emission lines, only the faint traces of the host galaxy and the galaxy marked with number 3 in figure 5.10. These traces are shown in figure 5.3. However, I find a possible [OII] emission line with a S/N of 5.68σ, corresponding to a redshift of $z = 1.6034 \pm 0.0001$ (see figure 5.4). This is consistent with the highest redshift intervening absorber. Since I can only find this one line, there is also the possibility of the line being another strong line of e.g. Hα, yielding a redshift of 0.4732 ± 0.0001.

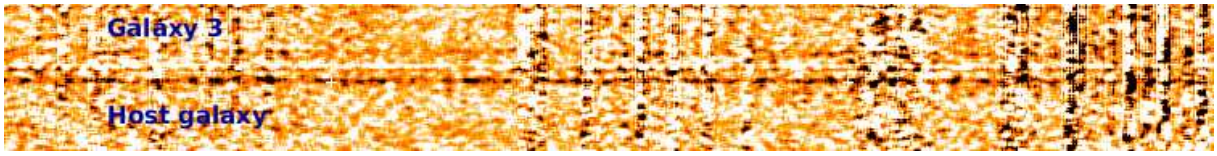

Figure 5.3: This figure shows two traces for position angle 30.50. The uppermost trace is for galaxy 3 and the bottom one is for the host galaxy.

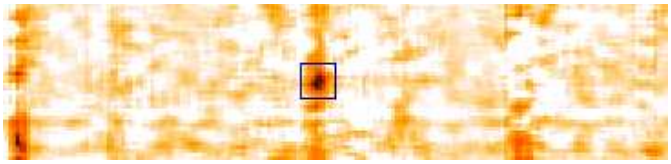

Figure 5.4: The possible [OII] emission line for galaxy 3. It is in the middle of a skyline and has a S/N of 5.68σ.

Table 5.1: The single [OII] emission line for galaxy 3 on the slit with position angle 30.50.

	λ_{rest} (Å)	λ_{obs} (Å)	z	S/N
[OII]	3727.26	9703.51 ± 0.50	1.6034 ± 0.0001	5.68σ

Position Angle 70.37

Figure 5.5 shows the 1D spectra for the position angle 70.37. For the upper trace I have found three emission lines of [OII]λ3727.26, NeIIIλ3869.84 and H$\delta\lambda$4102.90. The [OII] line is in the middle of skylines, which makes the S/N smaller. The redshift based on these lines is $z = 1.3849 \pm 0.0030$, which is consistent with the absorption system found by Møller et al. 2002b.

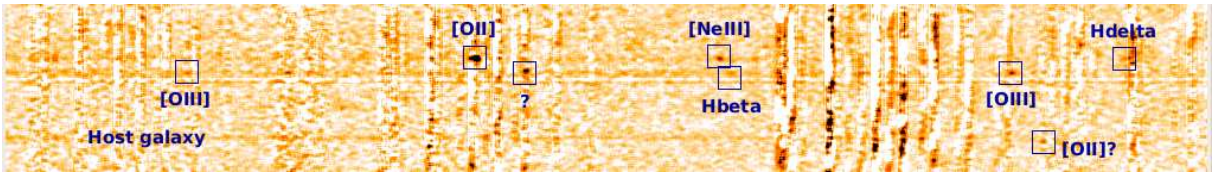

Figure 5.5: The traces of the galaxies in the environment of the GRB for position angle 70.37. I have marked the emission lines on the two upper traces as well as the single emission line just below the host galaxy.

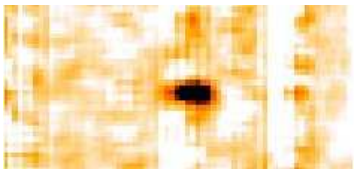

Figure 5.6: [OII] emission line for the $z = 1.3849$ galaxy.

Table 5.2: Emission lines for the uppermost trace on the slit with position angle 70.37.

	λ_{rest} (Å)	λ_{obs} (Å)	z	S/N
[OII]	3727.26	8891.63 ± 0.97	1.3856 ± 0.0003	9.21σ
[NeIII]	3869.84	9227.37 ± 0.28	1.3844 ± 0.0001	7.70σ
H_δ	4102.90	9783.96 ± 36.65	1.3846 ± 0.0089	2.27σ

Table 5.3: Possible emission lines for the galaxy placed right below the $z = 1.3849$ galaxy.

	λ_{rest} (Å)	λ_{obs} (Å)	z	S/N	Comment
[OIII]	4364.44	8497.54 ± 0.65	0.9470 ± 0.0001	1.46σ	Weak line in sky line
?	?	9242.13 ± 2.00	-	3.09σ	Weak line, far from sky lines
H_β	4862.70	9420.22 ± 1.28	0.9372 ± 0.0003	1.72σ	Placed in a sky line
[OIII]	4960.29	9627.05 ± 0.66	0.9408 ± 0.0001	6.16σ	Strongest line, close to sky line

For the trace just below the $z = 1.3849$ system, there seems to be two destinct emission lines at 9242.51 Å and 9626.59 Å, respectively, where the latter is the strongest. However these two lines together do not yield the same redshift. There are a couple of possible lines, but all of these are in skylines so they may not be lines at all. Based on these two they match with the strong line at 9626.59 Å and thus yield a redshift of $z = 0.9416 \pm 0.0001$. The lines are marked in figure 5.5.

The faint trace below this is from the host galaxy. Since the redshift of this is $z = 2.3351$ (Møller et al. 2002b), it will not be possible to see [OII] emission or any of the other metal lines longwards of this as they are outside of the wavelength range of the science frames.

Just below the trace of the host galaxy there is a possible emission line at λ9670.53 (see figure 5.7). This line has a S/N of 4.00σ. As there is no trace nor any other emission lines visible it could be caused by a faint galaxy where only one of the strong lines can be seen. If this is the [OII]λ3727.26 line, the redshift is $z = 1.5946 \pm 0.0002$, so this could be the intervening absorber at $z = 1.6039$. It might of course be another strong line instead from e.g. $H_\alpha\lambda$6564.63 in which case the redshift is $z = 0.4731 \pm 0.0001$.

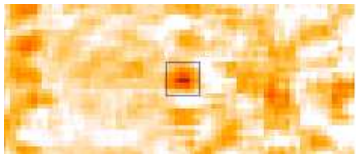

Figure 5.7: The single emission line for position angle 70.37 just below the host galaxy. This line might be [OII] emission.

Table 5.4: The single possible emission line at the position angle of 70.39.

	λ_{rest} (Å)	λ_{obs} (Å)	z	S/N
[OII]	3727.26	9670.69 ± 0.63	1.5946 ± 0.0002	4.00σ

5.1.2 Discussion

I found a galaxy at approx. the same redshift as the absorber at $z = 1.3806$. It is located 16" from the GRB host galaxy, corresponding to a radial distance of approx. 145 kpc (see figure 5.10). This galaxy was also found to have a redshift of $z = 1.38$ in the survey of Vreeswijk, Møller & Fynbo 2003. If this is in fact the absorber, it is consistent with the theory of the absorption being caused by large extended gaseous halos. There is of course still the possibility that this galaxy has the same redshift as the absorber by chance and is unrelated to the absorber. The actual absorber could be one of the faint galaxies at a smaller impact parameter which I have not been able to determine the redshift of. Comparing the determined redshift of $z = 1.3849$ with the $z = 1.3806$ absorption system yield a velocity distance of 512 km s^{-1}. This is a bit high, indicating that this galaxy has approx. the same redshift by chance and is unrelated to the absorber.

I actually found two possible single emission lines which might be from the absorber at $z = 1.6039$. The one at position angle 70.39 is perhaps the most interesting, as it has the smallest impact parameter of the two. If this is an emission line, the galaxy producing the line would lie at a distance of 0."75 corresponding to a radial distance of 6.8 kpc. Figure 5.8 shows a smoothed image of the GRB021004 host galaxy. This image was taken by the Hubble Space Telescope with an exposure time of 1920 s. I have marked where the single line emitting galaxy should be. However there are no visible object at this position. It is possible that the galaxy is simply too faint to be present in the image and as such falls below our detection limit in imaging for this frame. In this case a longer exposure time might reveal a galaxy. But it might also be that there simply is no galaxy present and what appears to be a line in the spectrum is caused by noise. I cannot verify whether the line is truly present as there is only one science frame. If I had had two frames I could have seen whether it was present on both. As the line is only 0."75 from host galaxy there is a possibility that it is present on the slit with position angle 91.41. In the combined science frame for this position angle the [OII] emission line would however be in the middle of a sky line and thus I cannot see any line there.

This [OII] line provides a redshift of $z = 1.5946$ and thus have a velocity distance of 1071 $\pm$ 23 km s^{-1} from the absorber. This is too large to be associated with the absorption system. Multiple science frames might also give a better determination of the redshift and might provide a redshift closer to the absorber. However, the descrepancy seen here, can most likely not be explained by a shift in the redshift determination. Even is this is an [OII] emission line, the galaxy producing it would most likely be unassociated with the absorption system.

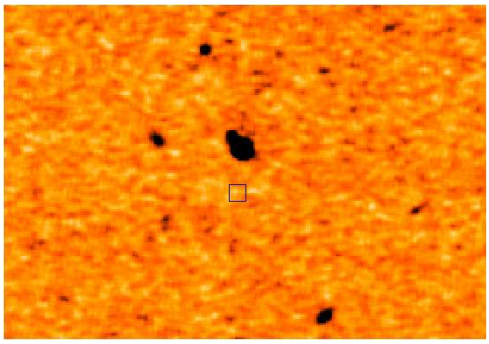

Figure 5.8: The hostgalaxy of GRB021004.

I also found a possible [OII] emission line for galaxy 3 yielding $z = 1.6034$. As this line is in the middle of a sky line it is a bit harder to say whether it is in fact an emission line or due to the skyline. However, the line has a S/N of 5.68σ which is high enough for the line to be significant. This indicates that the line is there. The spectrum containing this line is combined from four science frames. Thus I have tried to see whether the line is present in the single science frames. These are shown in figure 5.9. There is vaguely something visible that might show up as a line in the combined frame. Especially the two middle frames show a hint of a line.

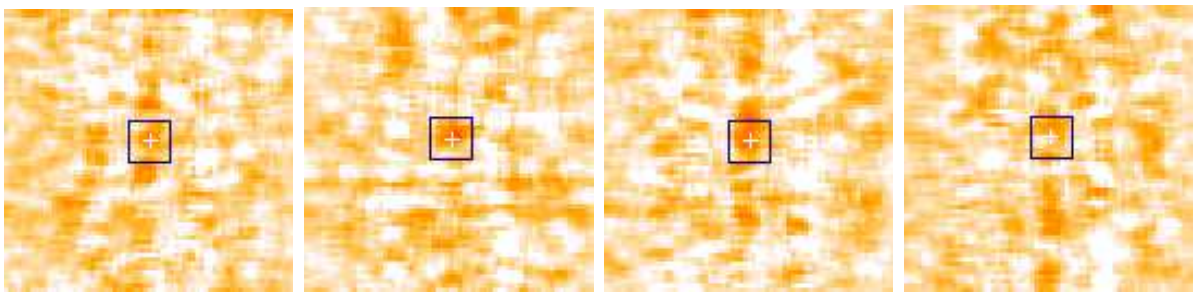

Figure 5.9: The single scienceframes before combining at the position of the possible [OII] line. There is vaguely something there, mostly for the two middle frames.

Galaxy 3 is 7" from the GRB021004 host galaxy corresponding to a radial distance of approx. 65 kpc (by assuming a flat Universe with $\Omega_m = 0.3$, $\Omega_\Lambda = 0.70$ and $H_0 = 65$ km s^{-1}Mpc^{-1}). Its velocity distance is only 58 ± 12 km s^{-1} compared to the absorber $z = 1.6039$ and thus this system is very likely the $z = 1.6039$ absorption system.

For the position angle 91.41 I have not been able to detect any lines. It is a possibility that the $z = 1.3806$ system is one of the galaxies covered by this slit and that the emission lines of galaxy 1 and 2 are simply too faint to detect. The only galaxy I have been able to determine the redshift of, besides the absorption systems, is the $z = 0.9416$ system. For this galaxy there is only one significant line, so the determination is uncertain. The distance to the GRB021004 host galaxy is 13.8" which corresponds to a radial distance of approx. 120 kpc. As this is not seen as an absorber it means we can constrain the halo size to 120 kpc.

There is also a galaxy within 5" which should have been covered by the slit with position angle 152.51. This is marked with number 4 in figure 5.10. However, no observations were made with this setup, so it is still not known whether this galaxy is the $z = 1.3806$ absorption system.

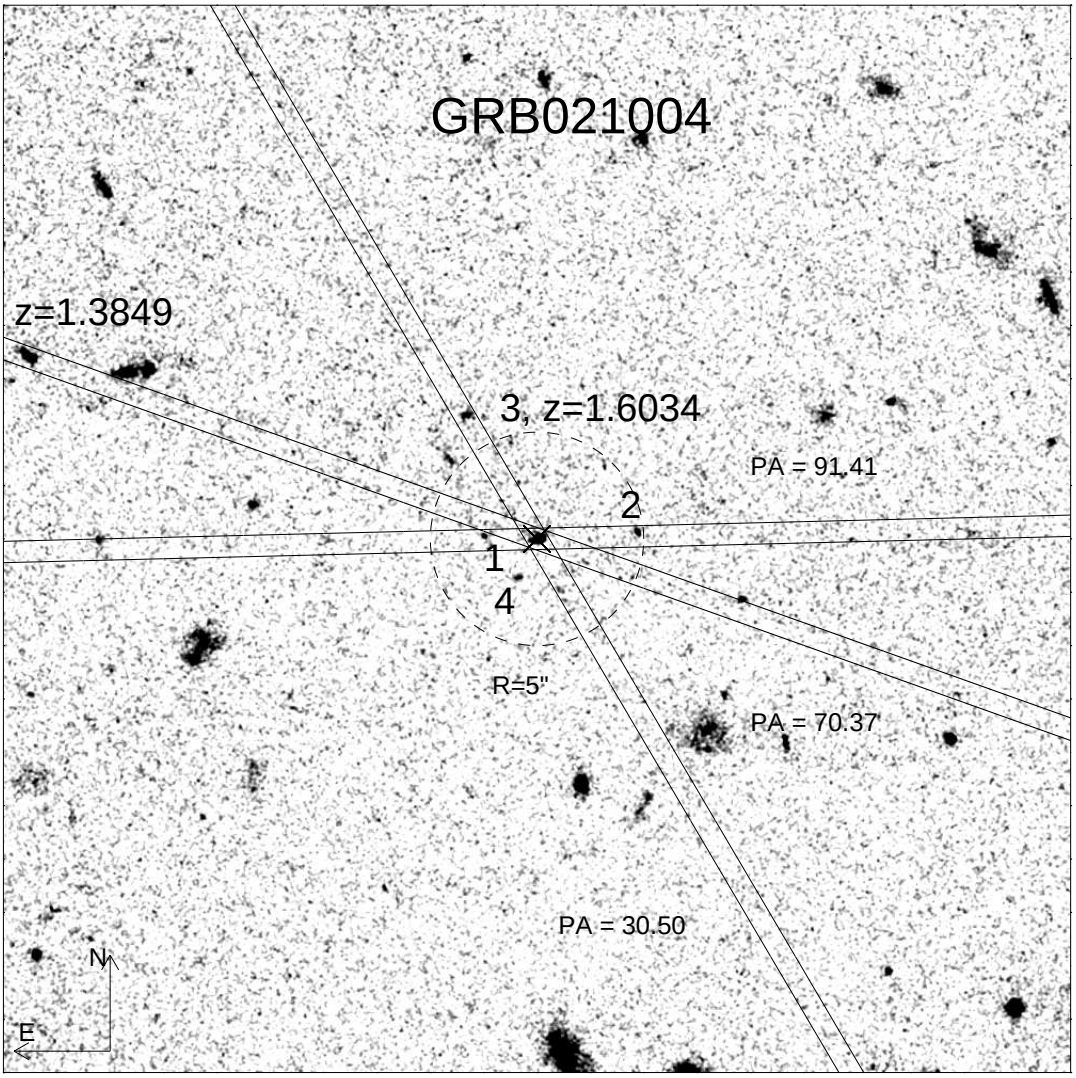

Figure 5.10: Measured redshifts of the galaxies in the field of GRB021004 at the three position angles.

5.2 GRB030226

GRB030226 has three absorption systems, where the two systems at $z = 1.963$ and $z = 1.986$ are in the GRB enivronment (see section 2.2.2) and the system at $z = 1.042$ is an intervening absorber. The observational setup provide a wavelength range of the science frames of approx. 5300 - 8630 Å. Thus the strongest observable lines at the redshift of the absorber at $z = 1.042$, are the [OII], [OIII] and H_β lines. The two other absorption systems cannot be determined on the basis of [OII] or Lyα emission as these lines fall outside the wavelength range of the science frames. There are several interesting galaxies in this GRB field which might be the intervening absorber (see section 3.2). There are two galaxies, one which is luminous, lying at a somewhat large impact parameter to the GRB. These are covered by the slits with the position angles 35.79 and 155.72. However the most interesting objects are the two faint galaxies at the position angle of 119.08, as these are both within a radial distance of 5" from the GRB site (see figure 5.15).

5.2.1 Emission Line Determination

Position Angle 35.79

For this position angle I only found one trace (see figure 5.11). This had two strong lines from [OII] and H_β respectively, yielding a redshift of $z = 0.7562 \pm 0.0001$. I have listed the lines in table 5.5. I found no other emission lines at a redshift of the absorber. The emission line in the upper left corner is most likely an [OII] line at a redshift of $z = 0.450$. A single line without a trace like this one, might also be a Lyα emitter. However, since these lines are usually extended, this is probably not the case here.

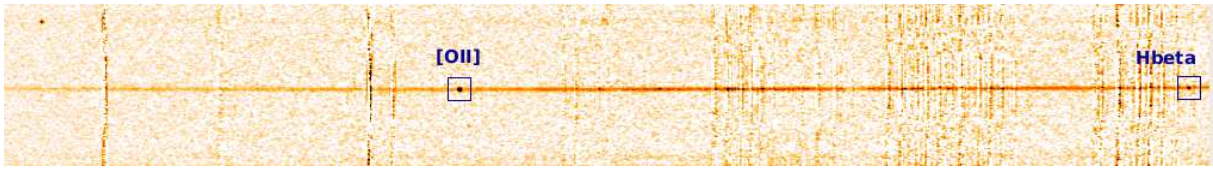

Figure 5.11: Trace for the galaxy at a slit position angle 35.79. The two identified emission lines of [OII] and H_β are marked with blue squares. The emision line that is seen over the trace of the galaxy in the left end of the spectrum, i.e. at lower wavelength, is possibly an [OII] line at $z = 0.45$.

Table 5.5: Emission lines for the galaxy placed on the slit with position angle 35.79

	λ_{rest} (Å)	λ_{obs} (Å)	z	S/N
[OII]	3727.26	6547.42 ± 0.49	0.7566 ± 0.0001	18.24σ
H_β	4862.70	8537.90 ± 0.37	0.7558 ± 0.0001	9.85σ

Position Angle 155.72

Here I found two traces, each with several emission lines making the redshift determination easy. These traces are shown in figure 5.12. For the uppermost trace I detected the lines of [OII], H_δ and H_γ. The redshift of this galaxy is $z = 0.9078 \pm 0.0002$. The bottom trace has four emission lines of [OII], [OIII] and H_β providing a redshift of $z = 0.4874 \pm 0.0001$. It is actually possible to see that this galaxy has an radial extension, as there is another faint trace just below with the same lines; these are just shifted a little bit to the right i.e. redshifted. This corresponds to a velocity distance of approx. 400 km s^{-1}. This extension of the galaxy can also be seen in figure 5.15. The wavelengths for all of these lines are shown in table 5.6.

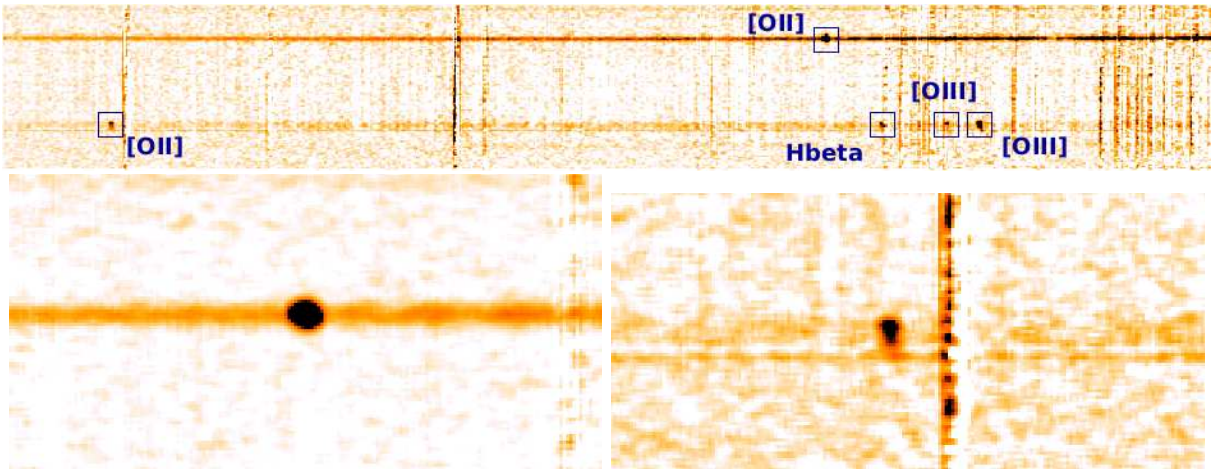

Figure 5.12: The upper panel shows the two traces for the position angle 155.72. I have marked some of the lines given in table 5.6. The lower two panels show the [OII] line for both galaxies. Left line has a S/N of 64.10σ and is for the upper trace. The right [OII] line, for the lower trace, has a S/N of 12.67σ. This line also show a radial extension of the galaxy producing the line.

Table 5.6: Emission lines for the two galaxies placed on the slit with position angle 155.72

	λ_{rest} (Å)	λ_{obs} (Å)	z	S/N
[OII]	3727.26	7112.11 ± 0.30	0.9081 ± 0.0001	64.10σ
H_δ	4102.90	7825.90 ± 2.75	0.9074 ± 0.0007	2.35σ
H_γ	4341.69	8282.94 ± 0.54	0.9078 ± 0.0001	4.62σ

	λ_{rest} (Å)	λ_{obs} (Å)	z	S/N
[OII]	3727.26	5545.83 ± 0.30	0.4879 ± 0.0001	12.67σ
H_β	4862.70	7232.26 ± 0.68	0.4873 ± 0.0001	18.75σ
[OIII]	4960.29	7377.25 ± 0.34	0.4873 ± 0.0001	3.74σ
[OIII]	5008.24	7448.25 ± 0.24	0.4872 ± 0.0001	10.32σ

Position Angle 119.08

This position angle was the most interesting one, but also turned out to be the less fruitful one, as I found no clear emission lines. Figure 5.13 shows the traces of these faint two galaxies which lie at a small impact parameter of the GRB. As is seen these traces are very faint and no evident emission lines are seen. The uppermost strongest trace is the galaxy marked in figure 5.15 as number 1. The lower is the one marked with number 2. I also checked to see whether small deviations, that would otherwise be regarded as noise, might be a faint emission line. However none of these would yield the redshift of the absorber. In figure 5.14 I have marked where [OII] emission should be from the $z = 1.042$ absorber. There are no lines present.

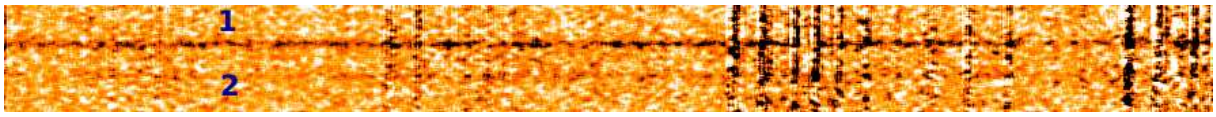

Figure 5.13: This is a spectrum for the position angle 119.08 where the traces of the faint galaxies within 5" of the GRB are. The top one is the strongest and the lowest is barely visible.

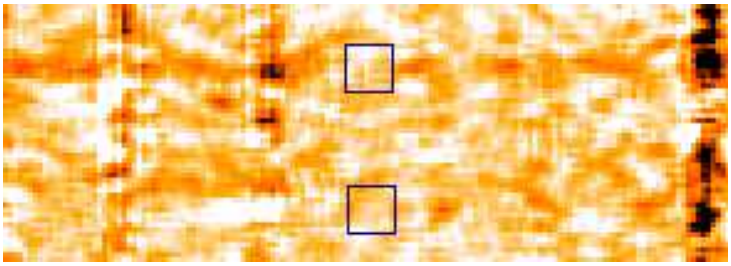

Figure 5.14: A zoom of figure 5.13 at the traces of galaxy 1 and 2. I have marked where the [OII] emission from the absorber at $z = 1.042$ should be.

Host Galaxy

To determine whether there might be an absorbing galaxy at an impact parameter of around 1", I have combined all the science frames from the three different position angles, by using a centering around the GRB site (see section 4.2.1). This might also reveal a possible trace of the host galaxy. However, I find neither a trace nor any emission lines there.

5.2.2 Discussion

I do not detect the absorption system at $z = 1.042$ in either of the slits. For the position angle 119.08, I do not detect any emission lines from the two galaxies within 5" of the GRB (see figure 5.15) and this can be due to a number of reasons. Either they fall below our detection limit (in which case we would need a longer integration time) or it could also be that these galaxies do not have any emission lines in the wavelength range of the science images. This also means that it is not possible to determine whether or not one of the two galaxies might be the host galaxy. It is worth noting that it is only the absorber at a redshift of 1.042 that can be detected in [OII] within the current wavelength range. This means that we can exclude the

presence of [OII] at this redshift. It is also interesting that there is no absorption of the galaxies at the lower redshifts in the spectrum of the optical afterglow of the GRB. This means that it is possible to put an upper constraint on the size of their halos. Assuming a flat universe with a matter density, $\Omega_m = 0.3$, a vacuum density of $\Omega_\Lambda = 0.7$ and a Hubble constant of $H_0 = 65$ $\mathrm{kms}^{-1}\mathrm{Mpc}^{-1}$, the upper limit to the radius of the haloes of the galaxies at z = 0.7562 and z = 0.9078 are 82 kpc and 68 kpc respectively.

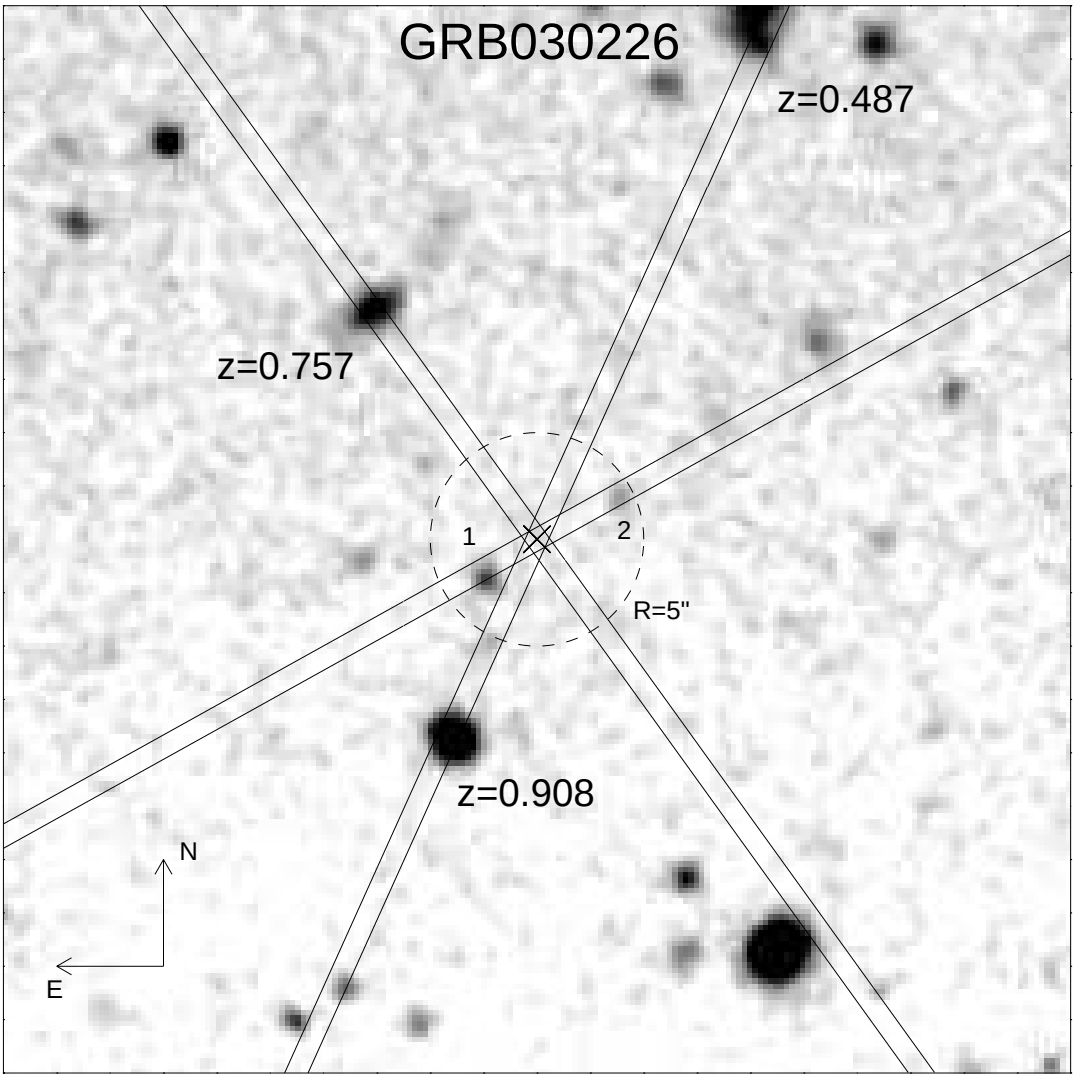

Figure 5.15: Measured redshifts of the galaxies in the field of GRB030226 at the three position angles.

5.3 GRB020813

This GRB has one strong intervening absorber at $z = 1.2234$. There are a couple of galaxies within 5" which are possible candidates for the galaxy counterpart. The host galaxy of GRB020813 is bright and should be present on all of the position angles. The redshift is 1.255 and was also seen in [OII]. The wavelength range of the science frames of 7730-9480Å permits a search for this [OII] emission of the host galaxy and I may thus verify the line as well as the redshift.

5.3.1 Emission Line Determination

Host Galaxy

The trace of the host galaxy stands out clearly (see figure 5.16) and shows two clear emission lines of [OII]λ3727.26 and [NeIII]λ3869.84, as well as two fainter lines of [NeIII]λ3970.00 and Hδ]λ4102.90. The [OII] line is so strong that it is possible to dissolve into two components (the [OII] line is a doublet). These lines yield a redshift of the host galaxy of $z = 1.2554 \pm 0.0001$.

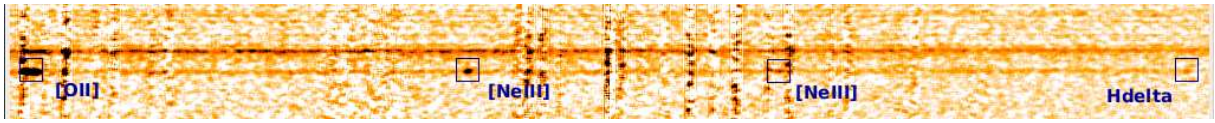

Figure 5.16: The trace of the GRB020813 host galaxy.

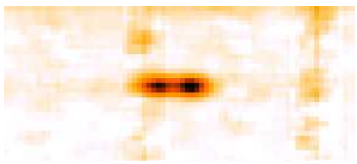

Figure 5.17: [OII] doublet emission line from the host galaxy.

Table 5.7: Emission lines for the GRB020813 host galaxy.

	λ_{rest} (Å)	λ_{obs} (Å)	z	S/N
[OII]	3727.26	8406.63 ± 0.33	1.2553 ± 0.0001	34.43σ
[NeIII]	3869.84	8725.70 ± 0.13	1.2548 ± 0.0001	17.83σ
[NeIII]	3970.00	8959.54 ± 0.25	1.2568 ± 0.0001	3.41σ
Hδ	4102.90	9250.47 ± 0.25	1.2546 ± 0.0001	5.78σ

Position Angle 27.00

There are three visible traces in this position angle, one of which is the host galaxy (see figure 5.18). There are no visible emission lines in the strong trace right above the host galaxy. In the trace below the host galaxy there is a possible line at 8636.70 Å with a S/N of 3.05σ. I cannot detect any other lines in this trace. Providing this line is [OII], the redshift is $z = 1.3172 \pm 0.0069$. Again there is a possibility that the line is something else, such as Hα. To see if there is [OII] emission present at the wavelength of the absorber, I zoomed in on this position for both of the visible traces (see figure 5.20). There are no lines present.

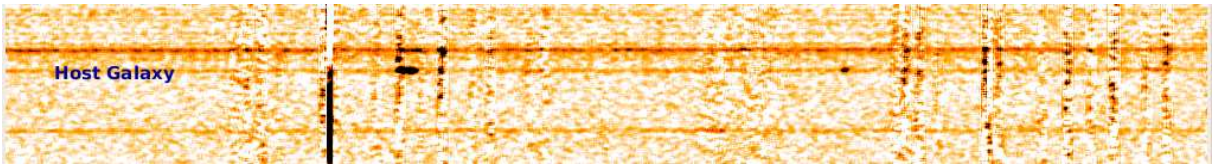

Figure 5.18: The visible traces on the slit with position angle 27.00.

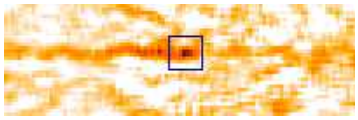

Figure 5.19: The possible [OII] emission line for the lowest trace.

Table 5.8: Possible [OII] emission line for the lowest trace in position angle 27.00.

	λ_{rest} (Å)	λ_{obs} (Å)	z	S/N
[OII]	3727.26	8636.70 ± 25.85	1.3172 ± 0.0069	3.05σ

Figure 5.20: Where the [OII] emission line of the absorber should be. Left Panel: For the visible trace above the hostgalaxy. Right Panel: The visible trace below the host galaxy.

Besides the visible traces, there are also two systems of emission lines, where no traces are visible. These are both above the host galaxy and are shown in figure 5.21. The lines present are e.g. the strong [OII] as well as [OIII] for the uppermost system on the slit (see table 5.9). On the basis of these lines the redshifts can be determined to be $z = 0.7276 \pm 0.0001$ for the uppermost system, and $z = 1.1137 \pm 0.0001$ for the lower.

Figure 5.21: The emission lines of in the slit of position angle 27.00. The lowest trace is the host galaxy, where the strong [OII] emission line is seen.

Table 5.9: Emission lines for the position angle 27.00.

	λ_{rest} (Å)	λ_{obs} (Å)	z	S/N
[OIII]	4960.29	8569.51 ± 0.11	0.7276 ± 0.0001	7.70σ
[OIII]	5008.25	8652.24 ± 0.11	0.7276 ± 0.0001	12.23σ

	λ_{rest} (Å)	λ_{obs} (Å)	z	S/N
[OII]	3727.26	7879.65 ± 0.22	1.1141 ± 0.0001	9.30σ
[NeIII]	3869.84	8177.70 ± 0.82	1.1132 ± 0.0002	6.07σ
Hγ	4341.69	9175.61 ± 2.19	1.1134 ± 0.0005	5.59σ
[OIII]	4364.44	9227.28 ± 0.39	1.1142 ± 0.0001	6.36σ

Position Angle 5.00

There is one strong trace visible for this position angle, besides the host galaxy. However, there are no visible emission lines, which is most likely due to no emission lines present in the wavelength range of the science frames. In figure 5.24 it is seen that this trace is caused by the galaxy which also cause the trace on the slit with position angle 27.00. For this position angle, no emission lines were found as well.

Position Angle -39.00

At this position angle, there is only one visible trace right above the host galaxy. In this trace there is a possible line in the middle of skylines at 8290.39 ± 0.98 Å. This might be [OII] emission, which would yield a redshift of $z = 1.2243 \pm 0.0001$, consistent with the redshift of the absorber. The shape of the line is somewhat distorted and does not look like [OII] emission normally looks. This effect might be caused by the skylines. There is also the possibility that what we see is noise in the skyline instead. However, given the S/N of 10.85σ, this is most likely an emission line.

Figure 5.22: Traces at the position angle -39.00. The buttom trace is from the host galaxy. The uppermost trace might contain an [OII] emission line yielding a consistent redshift with the absorber.

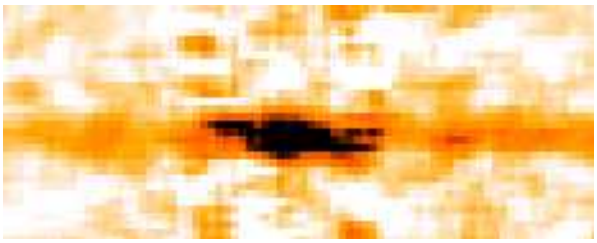

Figure 5.23: Possible [OII] emission from the galaxy right above the host galaxy on the slit. The line is quite elongated.

Table 5.10: The possible [OII] emission from the galaxy on slit position angle -39.00.

	λ_{rest} (Å)	λ_{obs} (Å)	z	S/N
[OII]	3727.26	8290.39 ± 0.98	1.2243 ± 0.0001	10.85σ

5.3.2 Discussion

There were many emission lines present in the trace of the GRB020813 host galaxy, making the redshift determination easy. I found this to be $z = 1.2554 \pm 0.0001$ which is consistent with previous studies. Fiore et al. 2005 determined the redshift to be $z = 1.255$, but does not have as many significant figures, thus further comparison does not make much sense.

I found one possible emission line which might be [OII] emission from the absorber, yielding a redshift of $z = 1.2243 \pm 0.0001$. When comparing to the redshift of the absorber at $z = 1.2234$ (Fiore et al. 2005), it is found that they are separated by 121 ± 13 km s^{-1}. Thus, this line is most likely caused by the absorber. The galaxy is 4.5" from the host galaxy which corresponds to 40 kpc and as such this is what I have been searching for.

There were several galaxies in the slit position angle 27.00, of which I was able to determine the redshift of. Two of these galaxies have redshifts lower than the GRB, i.e. at $z = 0.7276$ and $z = 1.1137$. As we do not see these as absorbers, the size of their halos must be smaller than 178 kpc and 100 kpc respectively.

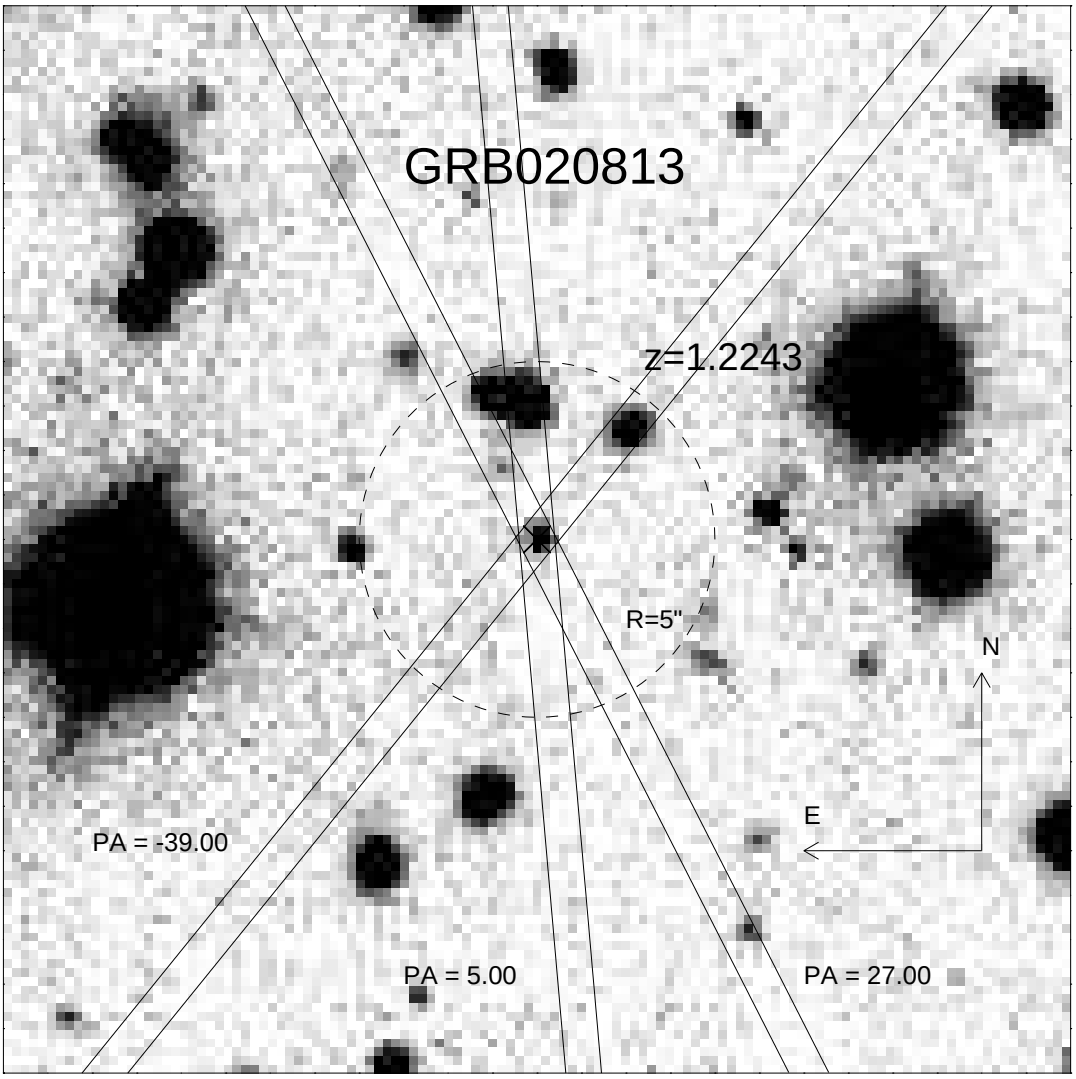

Figure 5.24: Measured redshifts for the field of GRB020813.

Chapter 6

Summary and Outlook

In this chapter I will summerize the results for the GRB fields as well as propose ideas for future work.

6.1 Summary

The aspect of this thesis work was to determine whether strong MgII absorption in GRB afterglows are associated with faint galaxies at small impact parameters.

Of my sample of three GRB fields, two revealed very interesting results. For both GRB021004 and GRB020813 I was able to find a possible galaxy counterpart for an absorption system. Both of the galaxies were found on the basis of the [OII]λ3727.26 emission line, with a significance of 5.68σ and 10.85σ respectively. The velocity seperation between the absorber and the proposed galaxy causing it, were in both cases small, i.e. approx. 60 km s^{-1} for the absorption system in GRB021004 and 120 km s^{-1} in the case of GRB020813. Velocity distances of this size, indicate that the found galaxies are most likely the absorbers. Thus absorbing galaxies might be found on the basis of [OII] emission, as has also been seen previously (e.g. Bergeron & Boisse 1991).

The most interesting is that the two galaxies are located fairly close to the GRB. The $z = 1.6034$ galaxy in the field of GRB021004 lies at a distance of 7" to the GRB sightline, corresponding to 65 kpc. For GRB020813, the $z = 1.2243$ galaxy is located 4.5" from the GRB, i.e. at a distance of approx. 40 kpc. Strong MgII absorbers have been believed to be associated with luminous galaxies at impact parameters up to several hundred kpc. However my work show that the absorbers might be found at much smaller impact parameters. This is especially evident for the absorption system in GRB020813, as this had the lowest distance of the two GRB fields. The search was aimed at finding the galaxy counterpart to absorption systems witin 5", so this system is what I have been looking for. The $z = 1.6034$ system in GRB021004 is, with the distance of 65 kpc, on the borderline between the two theories concerning large halos and faint galaxies at small impact parameters. However, it still shows that absorption galaxies might be found closer to 5" from the GRB, instead of the previously believed up to 12" (Bergeron & Boissé 1991). We are thus able to find the galaxies causing the absorption and are able to find them much closer than before.

The $z = 1.3806$ absorption system in GRB021004 has previously been associated with a galaxy at an impact parameter of 16" from the GRB (Vreeswijk, Møller & Fynbo 2003). My studies show that this galaxy is most likely not the absorber as I found a velocity shift of approx. 1070 km s^{-1} between this and the absorption system. There are also three galaxies within 5" that might be the possible absorber instead. Two of them were to faint for me to detect any lines and there had not been made any observations of the third galaxy.

I determined the redshift of several of the galaxies in the three GRB fields, which had a redshift lower than the GRB itself. As we do not detect these as absorption systems it means that the upper size of their halo can be constrainted. The galaxies in the field of GRB030226 had the lowest possible size of their halos, as their constraint was 68 kpc and 82 kpc respectively. It is interesting that these galaxies do not show up in the GRB spectra as absorbers, and these results are therefore in favor of the absorbers being galaxies at smaller impact parameters.

6.2 Outlook

There are several steps there might be taken in future research. I will now describe these.

Spectroscopic Follow-up

For GRB030226 I have not been able to find the intervening absorber. There are, however, two faint galaxies within an impact parameter of 5" which are possible candidates for the galaxy counterpart. It would be interesting to do a follow-up spectroscopic observation of these with an even higher exposure time in order to see whether any emission lines would become visible.

The same applies to GRB021004, as I have not found the $z = 1.3806$ absorption system. For this system there is also a possibility of the lines being one of three faint galaxies within 5" of the GRB. I was unable to determine the redshift of two of these, which might be because they fall below our detection limit. As such it would be interesting to find out if any lines might be present at higher exposures. Most of all, since I did not have any data for one of the position angles in this fiels, it would be interesting to carry out these observations, as the galaxy on this slit might be the absorber.

Future Research

As I have been able to associate absorbers with galaxies based on [OII] emission and at small impact parameters it seems that previous studies from QSOs have in fact missed these faint galaxies. Galaxies at small impact parameters for GRBs have been found by e.g. Jakobsson et al. (2004). However, no large surveys have been performed. It would be interesting to cover even more fields as this would provide us with not only a better sample but also the capability of determining whether faint galaxies at small impact parameters are detectable for most GRB fields.

Appendix A

Charged-Coupled Device

A Charged-Coupled Device (CCD) is an electrical device which collects the light from the sky and converts it to an electrical signal. It is constructed of a semiconducting material coated with a layer of metal oxide. When photons hit the CCD, electrons are liberated from the surface of the CCD. The quantum efficiency i.e. the ratio of electrons liberated per photon hitting the surface is usually about 0.70-0.80. The CCD is electrically charged which causes the electrons to travel into a potential well. This process will therefore imprint the difference in intensity of the incoming light by the number of electrons in each potential well. After an exposure the CCD can be read out. This is controlled by the electric potential on each pixel. By changing the applied voltage on the pixels it is possible to make the electrons move from one pixel to the one next to. Usually the lowest row is read out first, one pixel at the time, by use of an analog to digital converter (A/D). After this all of the above rows of the CCD are moved one row down and the whole procedure continues until the whole CCD is read out. When the data is passed from the hardware to a computers software the voltage measured for each pixel needs to be converted into a unit of counts. These are usually called Analog to Digital Units (ADUs) and provides a measure of the number of electrons on each pixel. The gain of the CCD connects the two and is given by the number of electrons per pixel devided by the number of counts per pixel (ADUs).

Several things can lead to noise on the CCD. During an observation where the CCD collects electrons the noise can come from thermal noise (dark current) or light pollution. The dark current can be minimized by cooling the CCD to low temperatures (this is usually done with liquid nitrogen). Another type of error comes when the CCD is read out. The read-out-noise (RON) is the extra number of electrons per pixel added when the CCD is read out and this is e.g. caused by the conversion from an analog to a digital signal and the electronics produce electrons which become part of the signal.

Appendix B

Command Lines

In this appendix I will give the most common types of command lines I used for the various reduction and analysis steps in *IRAF* and *IDL*.

B.1 Cosmic Ray Removal

The cosmic ray removal was performed in *IRAF* alone. The following is an example for one of the science frames.

```
stsdas

task lacos_spec=lacos_spec.cl

lacos_spec FORS2.2006-07-22T07:58:21.514.fits FORS2.2006-07-22T07:58:21.514out.f
its mask.pl gain=0.7 readn=2.9 xorder=9 yorder=25 niter=4
```

B.2 Image Reduction

The first part of the image reduction were to make a combined bias frame. I dit this by use of *IDL* where I made the following program:

```
PRO bias

xsize = 2048
ysize = 1034
nframes = 10
frame=''
n=0l
all_bias=FLTARR(xsize,ysize,nframes)
bias=FLTARR(xsize,ysize)

OPENR,u,'bias.list',/GET_LUN

WHILE NOT EOF(u) DO BEGIN
READF,u,frame
     a=READFITS(frame,header)
     overscan=MEAN(a(1:800,1030:1031))
```

```
     b=a-overscan
     all_bias(*,*,n)=b
     n=n+1
ENDWHILE

PRINT, "The median is calculated "

FOR i=0, xsize-1 DO BEGIN
     FOR j=0, ysize-1 DO BEGIN
             c = MEDIAN(all_bias(i,j,*))
             bias(i,j) = c
     ENDFOR
ENDFOR

PRINT, "The mean of the combined bias is ", MEAN(bias)

WRITEFITS, 'bias.fits', bias, header

CLOSE,u
FREE_LUN,u

END
```

After the combined bias frame is made the rest (bias subtraction from science frames and flatfielding) were done in *IRAF*.

```
ccdproc("b@.dump/allspectralist",ccdtype="",fixpix=no,overscan=yes,trim=no,zeroc
or=yes, zero="bias.fits",darkcor=no,flatcor=no,biassec=biassec,interac=yes,funct
ion="chebyshev",grow=1,readaxis=readaxis)
```

```
imcombine("b@"//flatlist0,output=".dump/flat",combine="median",scale="median",
statsec=flatsection)
```

```
response(".dump/flat",".dump/flat"//flatsection,".dump/nflat",low_rej=3.,high_
rej=3.)
```

B.3 Wavelength Calibration

This is an example for one of the slit position angles. cFORS2.2006-07-21T11:14:50.743.fits is the arc spectrum and cFORS2.2006-07-19T03:31:07.160out.fits is the combined science frame.

```
identify cFORS2.2006-07-21T11:14:50.743.fits coordlist=/home/chhe/work/tasks/myl
ines_vac.dat nsum=1 fwidth=8 cradius=8 maxfeatures=99 function=cheb order=4 zwid
th=18 autowrite+ threshold=300
```

```
reidentify cFORS2.2006-07-21T11:14:50.743.fits cFORS2.2006-07-21T11:14:50.743 ns
um=1 step=1 nlost=10 cradius=8 trace+ plotfile=do_reid_arc.gki
```

```
fitcoords cFORS2.2006-07-21T11:14:50.743 function=cheb xorder=6 yorder=3 plotfil
e=""
```

```
transform cFORS2.2006-07-19T03:31:07.160out.fits tFORS2.2006-07-19T03:31:07.160o
ut.fits cFORS2.2006-07-21T11:14:50.743 interp=spline3 flux+ logfiles="STDOUT,wlc
al_science.log"
```

B.4 Combining the Science Frames

For combining the frame shown here is the one with the reference at the lowest Y-position, hence the chosen cut in the frame.

```
imcopy tFORS2.2006-07-21T06:36:09.072out.fits[*,10:900] tmpimage1

imcalc tmpimage1,tmpimage2,tmpimage3,tmpimage4 tCombined_posang27 "im1+im2+im3+i
m4"
```

B.5 Background Subtraction and Smoothing

```
background tCombined_posang27 tCombined_posang27_b axi=2 int- fun=spline3 ord=5 nav
=1   low=3 hig=4.5 nit=4.5 sample="1:106,128:800"
```

Bibliography

Adelberger, K. L. et al. 2003, ApJ, 584, 45

Alvarez, M. A. & Abel, T. 2007, MNRAS, 380, 30

Barth, A. J. et al. 2003, ApJ, 584, L47

Bergeron, J. & Boissé, P 1991, A&A, 243, 344

Bouché, N., Murphy, M. T. & Péroux, C. 2002, MNRAS, 354, L25

Bouché, N., Murphy, M. T. & Péroux, C. 2007, astro-ph/0709.4248v2

Butler, N. R. et al. 2003, ApJ, 597, 1010

Campana, S. et. al. 2006, astro-ph/0611305

Chevalier, R. A. 2007, astro-ph/0706.0461v1

Davies, M. B. et. al. 2007, astro-ph/0704.1899v1

D'Elia, V. et al. 2006, arXiv (astro-ph/0609825)

Djorgovski, S.G., et al. 2002, GCN Circ. 1620

Fan, X. et al. 2001, AJ, 122, 2833

Fiore et al. 2005, ApJ, 624, 853

Fox, D. W 2002, GCN Circ. 1564

Fox, D. W. et al. 2003, GCN Circ. 1879

Fox, D. W. et al. 2003, Nature, 422, 284

Fox, D. W., Blake, C. & Price, P. 2002, GCN Circ. 1470

Francis, P. J., et al. 1991, ApJ, 373, 465

Frank, S. et al. 2006, astro-ph/0605676v2

Freedman, R. A & Kaufmann, W. J. III, 2001, Universe 6th Edition

Fynbo, J. P. U. 2000, PhD Thesis

Fynbo, J. P. U. et al. 2005, ApJ 633, 317

Fynbo, J. P. U. et al. 2006, astro-ph/0608313

Gehrels, N, Piro, L & Leonard, J. T. 2002, Scientific American

Guillemin, P. & Bergeron, J. 1997, A&A, 328, 499

Jakobsson, P. et al. 2004, A&A, 427, 785

Jakobsson, P. et al. 2005, MNRAS, 362, 245

Klebesadel, R. W., Strong, I. B., Olson, R. A. 1973, ApJ, 182, L85

Klose, S. et al. 2004, AJ, 128, 1942

Laursen, L. T. & Stanek, K. Z. 2003, 597, L107

Lazatti, D. et al 2002, A&A 396, L5

Longair, M. S. 1998, Galaxy Formation

Metzger, M. R. 1997, AUC, 6676, 3M

Mirabal, N. et al. 2003, ApJ, 595, 935

Møller et al. 2002a, ApJ, 574, 51

Møller et al. 2002b, A&A, 396, L21

Nemiroff, R. J. 1994, astro-ph/9402012

Nomoto, K. et al. 2007, astro-ph/0707.2219v1

Pandey, S. B. et al. 2004, A&A, 417, 919

Pedersen, K. et al. 2004, GCN Circ. 1924

Peterson, B. M. 1997, An Introduction to Active Galactic Nuclei

Porciani, C, Viel, M & Lilly, S. J. 2007, AJ, 659, 218

Prochaska, J. X. et al. 2004, ApJ, 611, 200

Prochter, G. E. et al. 2006, ApJ, 648, L93

Prochter, G. E., Prochaska, J. X. & Burles, S. M 2006, ApJ, 639, 766

Ryden, B. 2003, Introduction to Cosmology

Savaglio, S. et al. 2002, GCN Circ. 1633

Schaefer, B. E. et al. 2003, ApJ, 588, 387

Shin, M. et al. 2006, preprint (astro-ph/0608327)

Stahler, S. W. & Palla, F. 2004, The Formation of Stars

Steidel, C. 1995, astro-ph/9509098

Steidel, C. S. & Dickinson, M. 1992, ApJ, 394, 81

Steidel, C. S., Dickinson, M. & Persson, S. 1994, 437, L75

Sudilovsky, V. et al. 2007, astro-ph/0705.0706v2

Tejos, N. et al. 2007, astro-ph/0705.0387v1

van Dokkum, P. G. 2001, astro-ph/0108003

van Marle, A. J., Langer, N & Garcia-Segura, G 2007, astro-ph/0704.2073v1

Vreeswijk, P. M., Møller, P., Fynbo, J. P. U., 2003, A&A, 409, L5

Wolfe, A. M., Gawiser, E. & Prochaska, J. X. 2005, Ann. Rev. Astron. Astrophys., 43, 861

Watson, D. et al. 2007, astro-ph/0703678

Wolfe, A. M. et al. 1986, ApJ, 61, 249

Woosley, S. E. 1993, ApJ, 405, 273

Woosley, S. E. & Bloom, J. S. 2006, ARA&A, 44, 507

ESO-MIDAS User Guide 1998, ref. number: MID-MAN-ESO-11000-0003

FORS1+2 User Guide, 2006, ref. number: VLT-MAN-ESO-13100-1543